NONLINEAR FIBER MODELING OF STEEL-CONCRETE PARTIALLY COMPOSITE BEAMS WITH CHANNEL SHEAR CONNECTORS

A THESIS SUBMITTED TO
THE GRADUATE SCHOOL OF NATURAL AND APPLIED SCIENCES
OF
MIDDLE EAST TECHNICAL UNIVERSITY

BY

ALPER ÖZTÜRK

IN PARTIAL FULFILLMENT OF THE REQUIREMENTS
FOR
THE DEGREE OF MASTER OF SCIENCE
IN
CIVIL ENGINEERING

DECEMBER 2017

Approval of the thesis:

NONLINEAR FIBER MODELING OF STEEL-CONCRETE PARTIALLY COMPOSITE BEAMS WITH CHANNEL SHEAR CONNECTORS

submitted by **ALPER ÖZTÜRK** in partial fulfillment of the requirements for the degree of **Master of Science in Civil Engineering Department, Middle East Technical University** by,

Prof. Dr. Gülbin Dural Ünver
Dean, Graduate School of **Natural and Applied Sciences** _____

Prof. Dr. İsmail Özgür Yaman
Head of Department, **Civil Engineering** _____

Assoc. Prof. Dr. Eray Baran
Supervisor, **Civil Engineering Dept., METU** _____

Examining Committee Members:

Prof. Dr. Cem Topkaya
Civil Engineering Dept., METU _____

Assoc. Prof. Dr. Eray Baran
Civil Engineering Dept., METU _____

Assoc. Prof. Dr. Özgür Kurç
Civil Engineering Dept., METU _____

Assoc. Prof. Dr. Ozan Cem Çelik
Civil Engineering Dept., METU _____

Assist. Prof. Dr. Saeid Kazemzadeh Azad
Civil Engineering Dept., Atılım University _____

Date: ***December*** **14th, 2017**

I hereby declare that all information in this document has been obtained and presented in accordance with academic rules and ethical conduct. I also declare that, as required by these rules and conduct, I have fully cited and referenced all material and results that are not original to this work.

Name, Surname: Alper ÖZTÜRK

Signature:

ABSTRACT

NONLINEAR FIBER MODELING OF STEEL-CONCRETE PARTIALLY COMPOSITE BEAMS WITH CHANNEL SHEAR CONNECTORS

Öztürk, Alper

M. Sc., Department of Civil Engineering

Supervisor: Assoc. Prof. Dr. Eray Baran

December 2017, 58 pages

The purpose of this study is to develop a nonlinear fiber-based finite element model of steel-concrete composite beams. The model was developed in OpenSees utilizing the available finite element formulations and the readily available uniaxial material constitutive relations. The model employed beam elements for the steel beam and the concrete slab, while zero-length connector elements were used for the steel-concrete interface. The channel shear connector response used in numerical models was based on the previously obtained experimental response from pushout tests. Accuracy of the numerical models in predicting the response of composite beams with varying degree of composite action was verified with the results of the previously conducted composite beam tests. The response of composite beams was studied in terms of moment capacity, stiffness, cross-sectional strains, and interface slip. The slip behavior through the beam length was also verified with the analytical solutions in the literature. Progression of damage due to cracking and crushing of concrete slab as well

as tension and compression yielding of steel beam was studied in relation to the degree of composite action present. The numerically predicted response agreed well with the experimental results over the entire range of load-deflection curves for both the fully composite and partially composite beams. The numerical models were also able to accurately predict the interface slip between the steel beam and the concrete slab when compared to the experimentally determined slip values, as well as the closed-form slip predictions. Concrete cracking in slab was observed to start at very early stages of loading and progress very quickly irrespective of the degree of composite action. Concrete cracking was followed by the initiation of yielding at the bottom part of the steel beam. Yielding in the lower parts of the steel beam was observed to be more extensive in models with full composite action compared to the partially composite beams. The point that the initial portion of the load-deflection curve of composite beams deviates from linear response corresponded to the yielding of the entire bottom flange of steel beam.

Keywords: Channel Shear Connector, Composite Beam, Fiber Modeling, Finite Element Method, OpenSees

ÖZ

U PROFİL KAYMA BAĞLANTISI ELEMANLARI İÇEREN ÇELİK-BETON KISMİ KOMPOZİT KİRİŞLERİN DOĞRUSAL OLMAYAN FİBER METODUYLA ANALİZİ

Öztürk, Alper

Yüksek Lisans, İnşaat Mühendisliği Bölümü

Tez Yöneticisi: Doç.Dr. Eray Baran

Aralık 2017, 58 sayfa

Bu çalışmanın amacı, çelik ve beton kompozit kirişler için doğrusal olmayan fiber tabanlı bir sonlu eleman modeli geliştirmektir. Bu model, OpenSees programında halihazırda var olan sonlu eleman formülasyonları ve tek eksenli malzeme modelleri kullanarak geliştirilmiştir. Model beton döşeme ve çelik kiriş kısımlar için kiriş elemanlarından, arayüzde bulunan ve kayma bağlantılarını temsil eden elemanlar için ise sıfır uzunluklu bağlayıcı elemanlardan oluşmaktadır. Sayısal modelde kullanılan U-profil arayüz bağlantı elemanlarının tepkisi daha önce yapılan itme deneylerinin sonuçları baz alınarak oluşturulmuştur. Değişken kompozitlik oranına sahip olan sayısal modellerin güvenilirliği, daha önce yapılan kompozit kiriş testlerinin sonuçlarıyla doğrulanmıştır. Kompozit kirişlerin eğilme davranışları moment kapasitesi, rijitlik, kesit şekil değiştirmeleri ve arayüz kayması bakımından

incelenmiştir. Kiriş uzunluğu boyunca ölçülen arayüz kayması davranışı da literatürde yer alan analitik sonuçlarla doğrulanmıştır. Betonun çatlaması ve ezilmesi, çeliğin basınç ve çekme altındaki akması gibi hasar oluşumlarının ilerleyişi ve bu hasarların kompozitlik derecesi ile ilişkisi çalışılmıştır. Sayısal modellerin tahmin ettiği davranış, hem tam kompozit kirişler hem de kısmi kompozit kirişler için, deneylerden elde edilen yük-sehim eğrileri ile örtüşmektedir. Ayrıca, sayısal modellerden elde edilen arayüz kayması değerleri hem analitik tahminlerle hem de deneysel olarak belirlenmiş arayüz kayması değerleri ile örtüşmektedir. Betonun çatlaması yüklemenin çok erken aşamalarında gözlemlenmiş olup kompozitlik oranından bağımsız olarak hızlı şekilde ilerlemiştir. Beton döşemenin çatlamasını, çelik kirişin çekme bölgesinde akmaya başlaması takip etmiştir. Tam kompozit kiriş modelleri için çelik kiriş modelinin alt bölgesinin akması, kısmi kompozit modellerle karşılaştırıldığında daha fazla olduğu görülmüştür. Kompozit kirişlerin yük-sehim eğrilerinin doğrusal davranıştan saptığı nokta, çelik kirişin alt başlığının tamamının aktığı duruma karşılık gelmektedir.

Anahtar Kelimeler: Kompozit Kiriş, Fiber modelleme, OpenSees, U-Profil Kayma Bağlantısı, Sonlu Elemanlar Metodu

In memory of my grandmother, Zeynep ÖZTÜRK

ACKNOWLEDGEMENTS

I would like to appreciate my supervisor Assoc. Prof. Dr. Eray Baran for the continuous guidance and constructive criticism he has provided throughout the preparation of the thesis. Without his patience and encouragement, this thesis would not have been completed.

I would also like to express my sincere thanks to Dr. Cenk Tort for his suggestion and contributions especially dealing with the convergence problems throughout the analysis.

I am deeply grateful to my dearest mother Aydan Öztürk for her constant support and friendship.

I would like to give special thanks to my wife İpek Çakaloz Öztürk for her endless love, encouragement, support and letting me work in the living room.

Finally, I want to thank to my father R. Tezcan Öztürk who worked as a civil engineer in every piece of land from Maldives to Afghanistan for our family needs.

TABLE OF CONTENTS

LIST OF TABLES

TABLES

LIST OF FIGURES

FIGURES

CHAPTER 1

INTRODUCTION

1.1 COMPOSITE ACTION

Composite systems made of structural steel beams and reinforced concrete slabs have been widely used in buildings and bridges. Combination of these two materials to resist load effects allows utilizing a high bending capacity through compressive strength of concrete and tensile strength of steel. Such composite behavior results in structural efficiency by utilizing shallower beam depths, reduced live load deflections, increased span lengths, and stiffer floors. This also leads to an economy since design of light weight buildings can be achieved (Griffis, 1986).

The composite action combines the structural advantages of both steel and concrete materials as their combination leads to economical design. Figure 1.1 shows the strain variation throughout the cross section in the absence and presence of composite action between neighboring layers. In the case of a fully composite behavior no slip is expected to occur between the two media and hence the section behaves like a single continuous material. However, when there is no or insufficient bond between the neighboring layers the strain distribution of each layer becomes independent. Partial shear connection is somewhere between the full composite and non-composite action where there exists a partial connection between the two media.

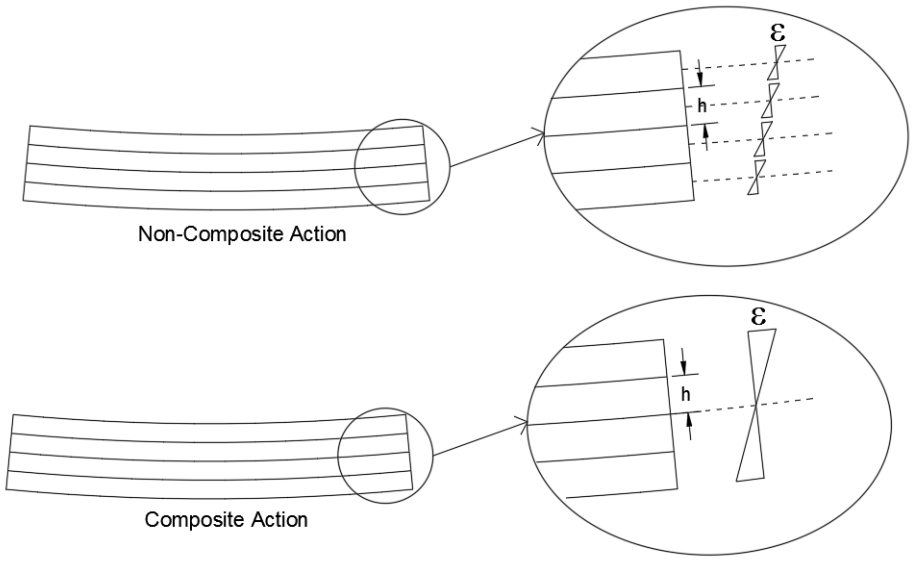

Figure 1.1. Difference between composite and non-composite action

Composite beam response is typically dominated by the degree of the composite action, which depends on the number of mechanical connectors provided at the interface as well as the shear strength of each connector. Degree of composite action is defined as the ratio of the total horizontal shear capacity of connectors in a shear span to the smaller of the yield capacity of steel section and the crushing capacity of the concrete slab. The designer often has the flexibility to determine the required degree of composite action. Even though a full composite action would result in a larger load capacity and stiffness, a partially composite action may offer a more economical design, simply because a reduction in the number of mechanical shear connectors can be achieved.

Composite action between the concrete slab and the steel beam is usually provided by limiting the relative displacement between the two media through embedded connectors since the frictional and chemical bonds at the interface are usually weak. Using a mechanical connector ensures that there is at least a partial restraint that prevents slip to a certain extent depending on the deformation behavior of the connector.

The internal force effects that will develop at steel-concrete interface in a composite beam subjected to flexural loading are shown in Fig. 1.2. As illustrated in

the figure, slip and uplift demands usually occur at the interface. The slip demand creates horizontal shear force and uplift demand creates tensile force in shear connectors. Therefore, in order for the member to exhibit a composite response these shear and tensile force demands must be met by the shear connectors. In other words, shear connectors with sufficient strength and stiffness to resist these effects must be provided at the interface.

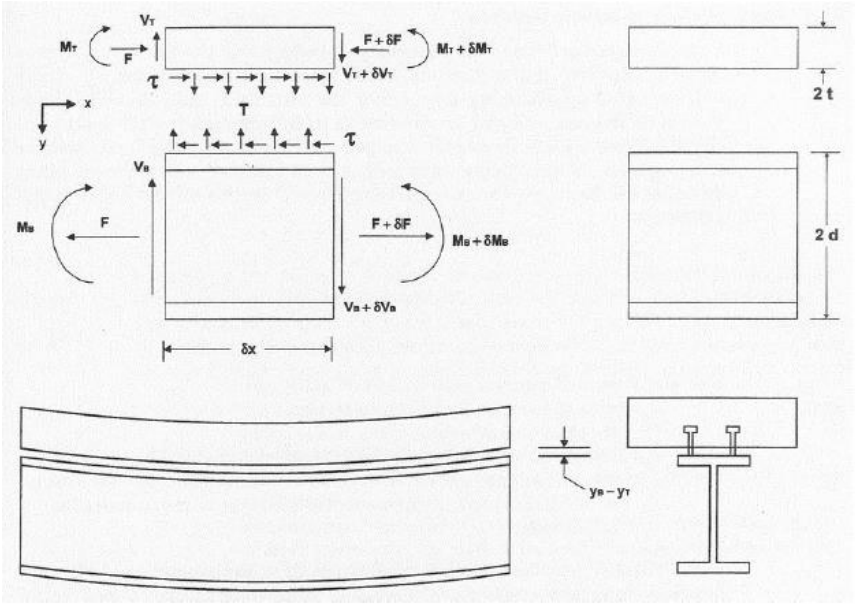

Figure 1.2. Forces acting on a composite beam under pure bending (Viest et al., 1997)

1.2 DEGREE OF COMPOSITE ACTION

Degree of composite action is a major concept for the design of composite beams and has a significant effect on the flexural response of a composite beam. Degree of composite action can simply be defined as the ratio of total horizontal shear capacity of connectors in a shear span to the smaller of yield capacity of the steel beam and crushing capacity of the concrete slab:

$$\text{Degree of Composite Action} = \frac{\sum Q_n}{\min(A_s F_{y,} 0.85 f'_c A_c)} \qquad \text{(Eq. 1.1)}$$

where $\sum Q_n$ is the total horizontal shear capacity, A_s is the area of the steel beam, F_y is the steel yielding strength, f'_c is the concrete crushing strength and A_s is the concrete slab area.

The degree of interaction between the steel beam and concrete slab determines the strain profile across the cross section of a composite beam, as illustrated in Fig. 1.3. Any slip that may take place at steel-concrete interface decreases the composite action. Presence of such interface slip leads to a discontinuous strain profile through the composite section with a sudden strain change at the interface location. For sections with no interface slip between the steel beam and concrete slab, the case of full interaction is obtained. In this case the cross-sectional strain profile becomes continuous with the steel and concrete strains equal to each other at the interface. As evident in Fig. 1.3, the cross section has a single neutral axis when a full interaction is obtained.

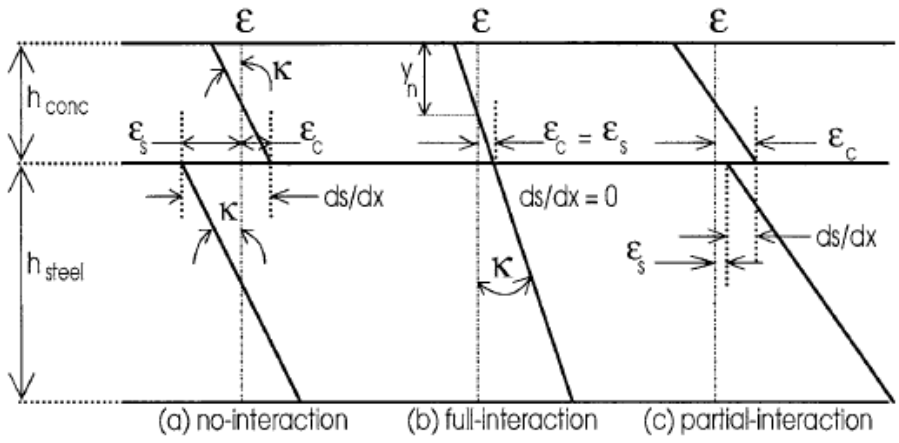

Figure 1.3. Degree of interaction between steel and concrete in a composite beam cross section (Oehlers and Bradford, 1995)

1.3 SHEAR CONNECTOR TYPES

In the market, the most common type of mechanical connectors is the headed shear studs. These studs are often attached to the top flange of beams through arc welding. Despite the economy and ease of application offered by the headed shear studs, there are many connector types that can also be used as a practical alternative. Several different types of mechanical shear connectors, including angle, T-shaped, channel, headed studs and bolts, are shown in Fig. 1.4. New types of connectors are being increasingly used and experimental studies are carried out to obtain better alternatives to the headed shear connectors. Among these new types of mechanical connectors, perfobond ribs and oscilating perfobond strip type of shear connectors can be given as interesting examples. These connectors include a welded steel plate with number of holes left on them, as shown in Fig. 1.5. In this system, transverse rebars go through the holes located on the steel plate and the force transfer between the steel beam and the concrete slab is achieved through these rebars.

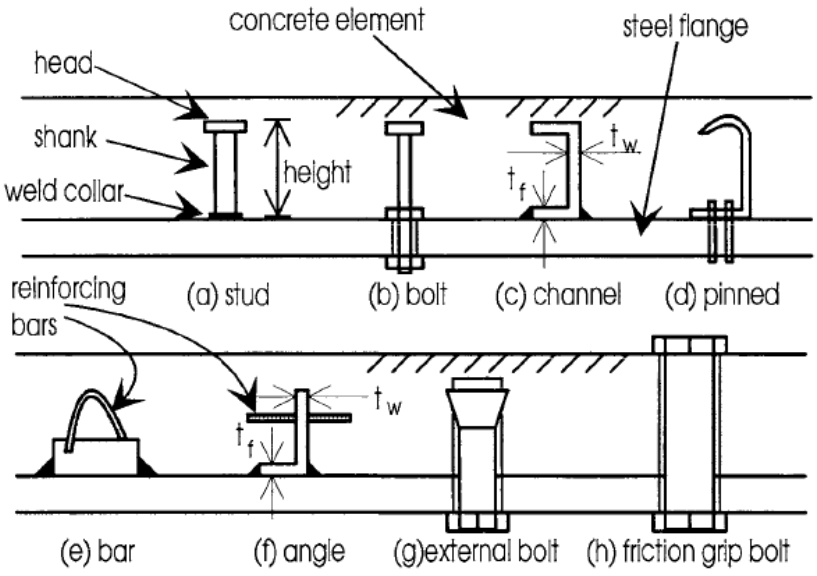

Figure 1.4. Mechanical shear connectors (Oehlers and Bradford, 1995)

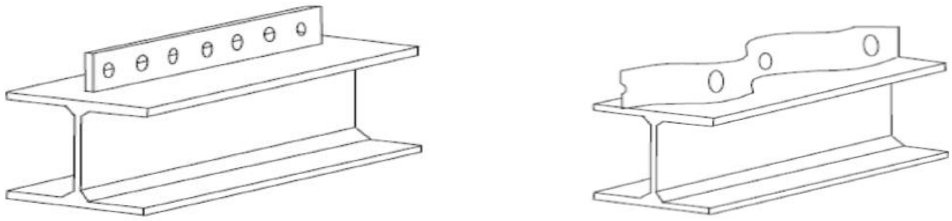

Figure 1.5. Perfobond ribs and oscilating perfobond strip shear connector (Muhit, 2015)

As mentioned in previously, channel shear connectors can be considered as a viable alternative for the conventionally used mechanical connectors. Some examples of the use of mechanical shear connectors made of channel sections in composite structural systems are provided in Fig. 1.6. One of the major advantages of this type of connectors over headed shear studs is that the required interface shear capacity can be met with fewer connectors by properly sizing each channel connector (Baran and Topkaya, 2012; Viest et al., 1952; Pashan and Hosain, 2009; Maleki and Bagheri, 2008). The fact that channel shear connectors can be attached on steel beams using conventional welding equipment is another major benefit of these connectors (Fig. 1.7). It should be noted that the use of headed studs requires special welding equipment that needs high voltage for operation (Fig. 1.8). Due to their superior features, the use of channel shear connectors on steel-concrete composite systems has been gaining popularity. Provisions on the use of channel shear connectors are also available on design codes. For example, North American Steel Design Specifications (AISC, 2010; CSA, 2001) include analytical methods to determine the load capacity of channel shear connectors.

(a)

(b)

(c)

Figure 1.6. Examples of mechanical shear connectors made of channel sections

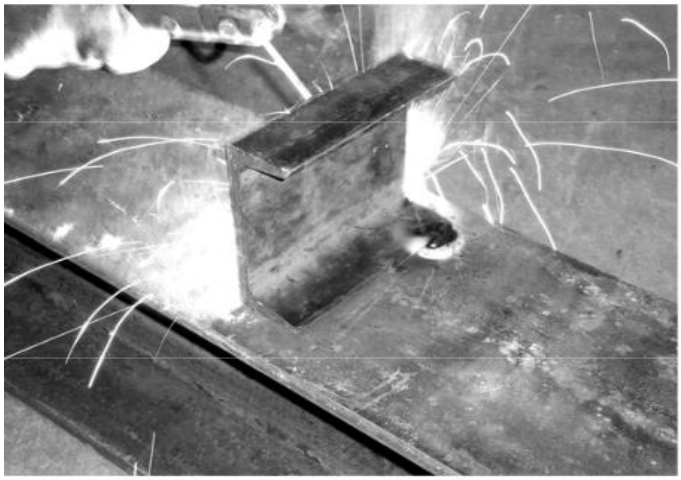

Figure 1.7. Channel shear connector welded to beam flange (Pashan, 2006)

Figure 1.8. Welding of stud shear connector using a welding gun (Pashan, 2006)

1.4 LITERATURE REVIEW

Numerical analysis of the flexural behavior of composite beams with headed shear studs, as well as the pushout response of these studs has been studied extensively through finite element modeling. Three-dimensional modeling of pushout tests was previously conducted both for conventional and large size headed shear studs. Queiroza et al. (2007) conducted 3D finite element modeling of simply supported

composite beams under uniform and concentrated loading using shell, solid and nonlinear spring elements in a commercial finite element software. All key nonlinear phenomena of yielding, cracking, crushing and slip were captured. A parametric study was also conducted to assess the structural performance against the degree of composite action, concrete strength and extent of shear connectors. Accurate correlations between experimental and computational results were presented. Lin and Yado (2014) studied the nonlinear response of composite beam sections of curved bridges. The analysis model was developed using a commercial software. The concrete slab, steel beam and shear connectors were simulated by solid, shell and spring finite elements, respectively. A nonlinear interface was also introduced to model the interaction between steel and concrete. The evolution of neutral axis of both steel and concrete was monitored. Lam and Lobody (2005) presented a computational study on modeling of headed shear studs in pushout tests. The results of the model were verified with experiments. A parametric study was also conducted in order to assess the accuracy of the European and American design specifications in predicting the shear capacity of different diameter headed studs. Practical methods for inelastic analysis of partially composite steel-concrete beams have been developed by Chiorean et al. (2017). These practical formulations were implemented into a general nonlinear static analysis software. The experimental observations and the practical inelastic analysis results were compared with other advanced finite element analysis results in the literature. Dall'Asta and Zona (2002) numerically investigated the partial composite action behavior by varying the number of the shear studs. In order to capture the partially composite behavior, three different element formulations were given using elements with eight, ten and sixteen degrees of freedom. The numerical results were compared with two-span composite steel-concrete beams tested up to failure. It was concluded that the correlation between the experimental and numerical results is improved as the degrees of freedom used for the elements increase. It was also reported that the convergence criteria needs to be studied carefully due to non-linearity in the partially composite beam problem. Salari et. al. (1998) developed a force-based non-linear element formulation. The load-deflection and moment-curvature relations of displacement-based and force-based elements were compared. For force-based elements, the bonding force distribution along the elements were implemented by

cubic polynomial shape functions. In the force-based formulation, the shape functions for the internal forces were selected as fourth-order. A simply supported composite beam was analyzed under pure bending and three-point bending conditions. The force-based formulation was reported to produce more accurate results than the displacement-based formulations. This result was attributed to better representation of curvature under nonlinear conditions with a force-based formulation. Rios et al. (2017) developed a finite element model considering the non-linear shear-bond behavior and introduced radial-thrust element connectors extending along the steel-concrete interface. The numerical results were compared with four-point and six-point bending tests. The results proved the accuracy of the model to simulate the response of composite slabs. Wang et al. (2017) derived a simplified analytical solution for simply supported steel-concrete composite beams based on a partial differential equation. The solution was tested for both three-point bending and uniformly distributed loading conditions. It was reported that the proposed solution produced accurate results considering the interfacial slip and shear deformation of the steel.

The use of cold-formed steel members in composite floor systems has also been the subject of research studies. Majdi et al. (2014) conducted finite element analysis of light-gage steel profiles in a system made of corrugated steel deck as slab formwork and a continuous hat channel as shear connector. The model results were compared with the experimental data and parametric studies were done to investigate the ultimate strength and initial stiffness of the system.

Higgins and Michell (2001) tested composite bridge decks using alternative mechanical shear connectors which consist concrete filled holes in structural steel sections. Shear transfer between concrete slab and steel grid is provided by these concrete dowels passing through the holes located in the webs of the main plates.

Studies are also available in the literature on chemical bonding to ensure composite action. Instead of using mechanical connectors, it is possible to utilize epoxy in order to provide connection between steel and concrete. Jurkiewiez et al. (2014) modeled epoxy bonded beams by using multi-layered beam model that takes into account the redistribution of stresses when a concrete layer cracks. Ranzi and Zona (2007) presented an analytical model for composite behavior of steel-concrete

composite beams taking into account the shear deformability of the steel component using Timoshenko beam formulation. Using virtual work principle and linear elastic properties of the two materials, several simply supported and continuous beams were studied. Redistribution due to time dependent behavior of the concrete was also modeled using a general linear visco-elastic integral type constitutive law. The results revealed that shear deformations need to be evaluated in detail particularly in the case of continuous beams. As another alternative to mechanical shear connectors, Jurkiewiez et al. (2011) studied the nonlinear behavior of steel-concrete epoxy bonded composite beams and reported that this connection type behaviour is very similar to composite beam with mechanical connectors where the bonding joint needs to be designed properly.

Several researchers also studied the response of channel shear connectors and that of steel-concrete composite beams. Maleki and Bagheri (2008, 2009) investigated the pushout response of channel shear connectors both experimentally and numerically. Contact elements were used to model the interface between steel beam and concrete slab, as well as between the channel connectors and the surrounding concrete. Parametric studies showed that channel connector capacity is related with the concrete strength, web and flange thickness of the connector, as well as the channel length. It was concluded that the channel height has no significant effect on the pushout response. Shariati et al. (2011) tested channel shear connectors to investigate the shear resistance using three different concrete types of lightweight, plain, and reinforced concrete. It was concluded that the performance differs as the length of the channel connector changes, with the larger connector length resulting in more cracking in concrete slab. It was also reported that the lightweight concrete has adequate performance to be used in composite structures with channel shear connectors. Pashan and Hosain (2009), performed push-out tests by varying the channel length, channel web thickness and concrete strength. It was stated that having longer channel length improves both ductility and strength of the channel connector. The concrete strength was reported to have an impact on the failure pattern. In the case of higher strength concrete the governing failure mode was observed to be channel web fracture, while concrete crushing and splitting type failures were observed when lower strength concrete was used.

The main aim of this study is to develop a 2D non-linear fiber model and investigate the flexural response of the composite beams with channel shear connectors. Previous studies for composite beams with channel shear connectors were three-dimensional finite element simulations of the tests. Instead a simpler, an easy to track, two-dimensional model was developed. The contribution of this study to the state of the art is to identify the relation of the partial composite action with flexural response in composite beams with channel shear connectors.

1.5 TESTS ON CHANNEL SHEAR CONNECTORS AND PARTIALLY COMPOSITE BEAMS BY BARAN AND TOPKAYA (2012, 2014)

The benchmark problem of this work is based on two previous studies. The first one investigated the transverse load-slip behavior of channel type mechanical shear connectors. Push-out tests were conducted on five different types of European channel type sections namely UPN65, UPN80, UPN100, UPN120 and UPN140 (Baran and Topkaya, 2012). The investigated parameters were the channel depth and length. The heights of the sections range from 65 to 140 mm and the channel lengths were 50, 75 and 100 mm. The specimen dimensions are shown in Table 1.1.

Among the 15 pushout tests conducted as part of the study 13 of them were with a single shear connector and the remaining two were with double shear connectors. The specimen details related with the pushout tests are given in Fig. 1.9. The load-slip response obtained from these pushout tests were used to describe the nonlinear material behavior of the channel connectors utilized in the current numerical study. After introducing the material parameters for the numerical model of the mechanical shear connectors, these connectors were then implemented into the beam finite element models simulating the behavior of the partially composite beams.

As part of the investigation focusing on the behavior of partially composite beams utilizing channel type shear connectors, monotonic three-point load testing of seven full-scale beams was conducted by Baran and Topkaya (2014). Six of the beam

specimens had different levels of composite ratio while one specimen was a steel beam with no concrete slab. Details of the beam specimens are summarized in Table 1.2.

Table 1.1. Properties of channel specimens tested by Baran and Topkaya (2012)

Specimen	**Number of channel connectors**	**Channel size**	**Channel height, H (mm)**	**Channel length,Lc (mm)**	**Concrete strength, f'c (MPa)**
S65-50	1	UPN 65	65	50	31.8
S80-50		UPN 80	80	50	33.3
S100-50		UPN 100	100	50	32.2
S120-50		UPN 120	120	50	39.9
S140-50		UPN 140	140	50	36.7
S65-75		UPN 65	65	75	34.7
S80-75		UPN 80	80	75	33.8
S100-75		UPN 100	100	75	36.7
S120-75		UPN 120	120	75	32.7
S140-75		UPN 140	140	75	32.9
S65-100		UPN 65	65	100	34.0
S80-100		UPN 80	80	100	34.5
S100-100		UPN 100	100	100	33.4
D65-50	2	UPN 65	65	50	34.6
D80-50		UPN 80	80	50	33.9

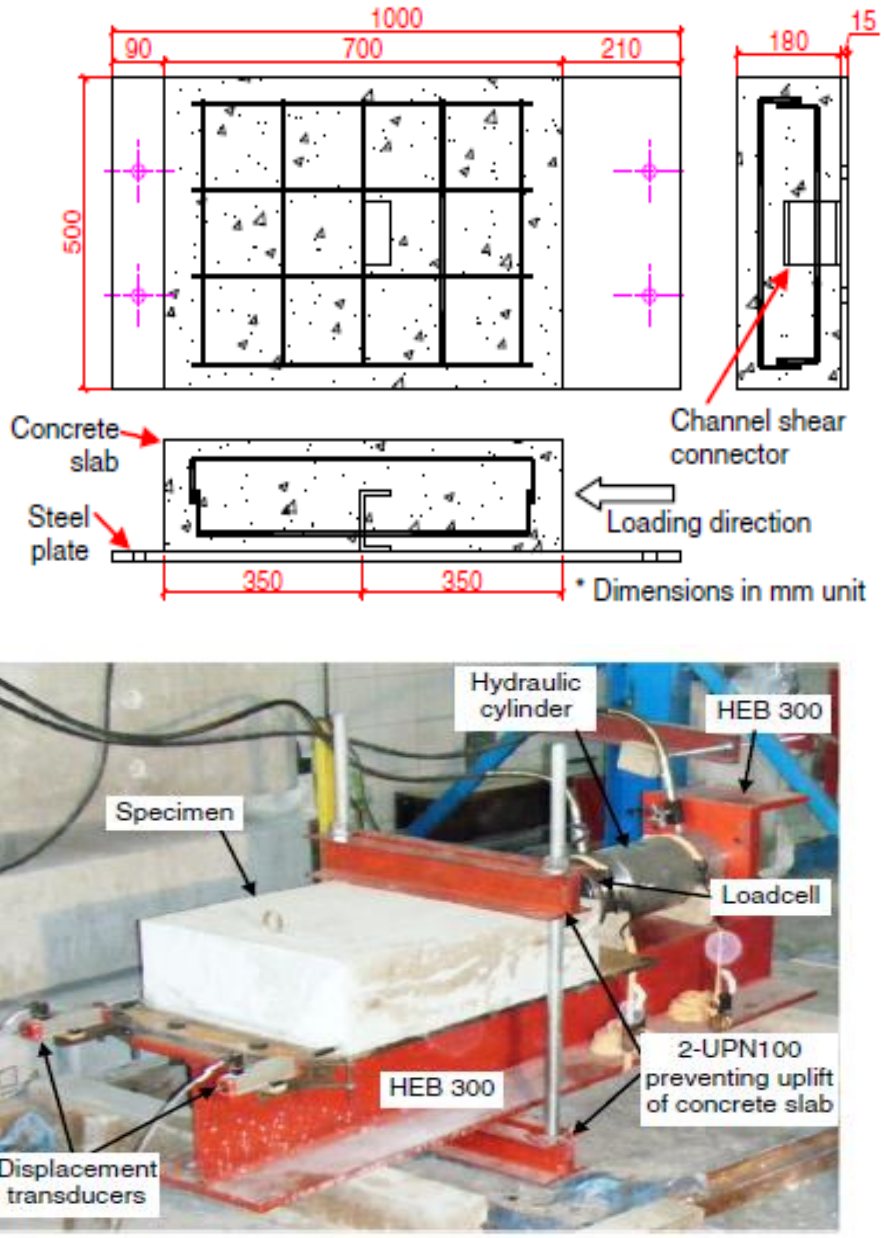

Figure 1.9. Details of specimen and setup for pushout tests by Baran and Topkaya (2012)

Table 1.2. Properties of beam specimens

Beam Specimen	Number of shear connectors per shear span	Shear connector type	Shear connector length, mm	Degree of composıte action
Bare Steel	-	-	-	-
2-UPN65x50	2	UPN65	50	0.35
3-UPN65x50	3	UPN65	50	0.53
4-UPN65x50	4	UPN65	50	0.70
6-UPN65x50	6	UPN65	50	1.06
4-UPN65x100	4	UPN65	100	1.04
5-UPN65x75	5	UPN65	75	1.19

Beams were tested under monotonically increasing vertical displacement loading applied at the centerline of a 360 cm span, as indicated in Fig. 1.10. The composite specimens consist of European section IPE240 beam and a 80 cm wide and 10 cm thick concrete slab. A relatively narrow concrete slab was placed on steel beams so that entire width of the slab could contribute to load resisting mechanism. The concrete slab was reinforced with a single layer of steel mesh. The degree of composite action was altered by changing number and length of the channel connectors per shear span. The measured concrete compressive strength values varied between 32.6 and 33.8 MPa. The yield strength of steel beams was determined by taking coupon samples from webs and flanges of the steel beams. Results of these tests revealed that yield strength of the web is 315 MPa and the ultimate strength is 466 MPa. The concrete slab was reinforced with a steel mesh of 10 mm diameter steel bars at spacing of 12 cm in longitudinal and transverse directions. Clear cover was 2.5 cm from the bottom surface of the slab. The yield strength of the steel rebars were 420 MPa.

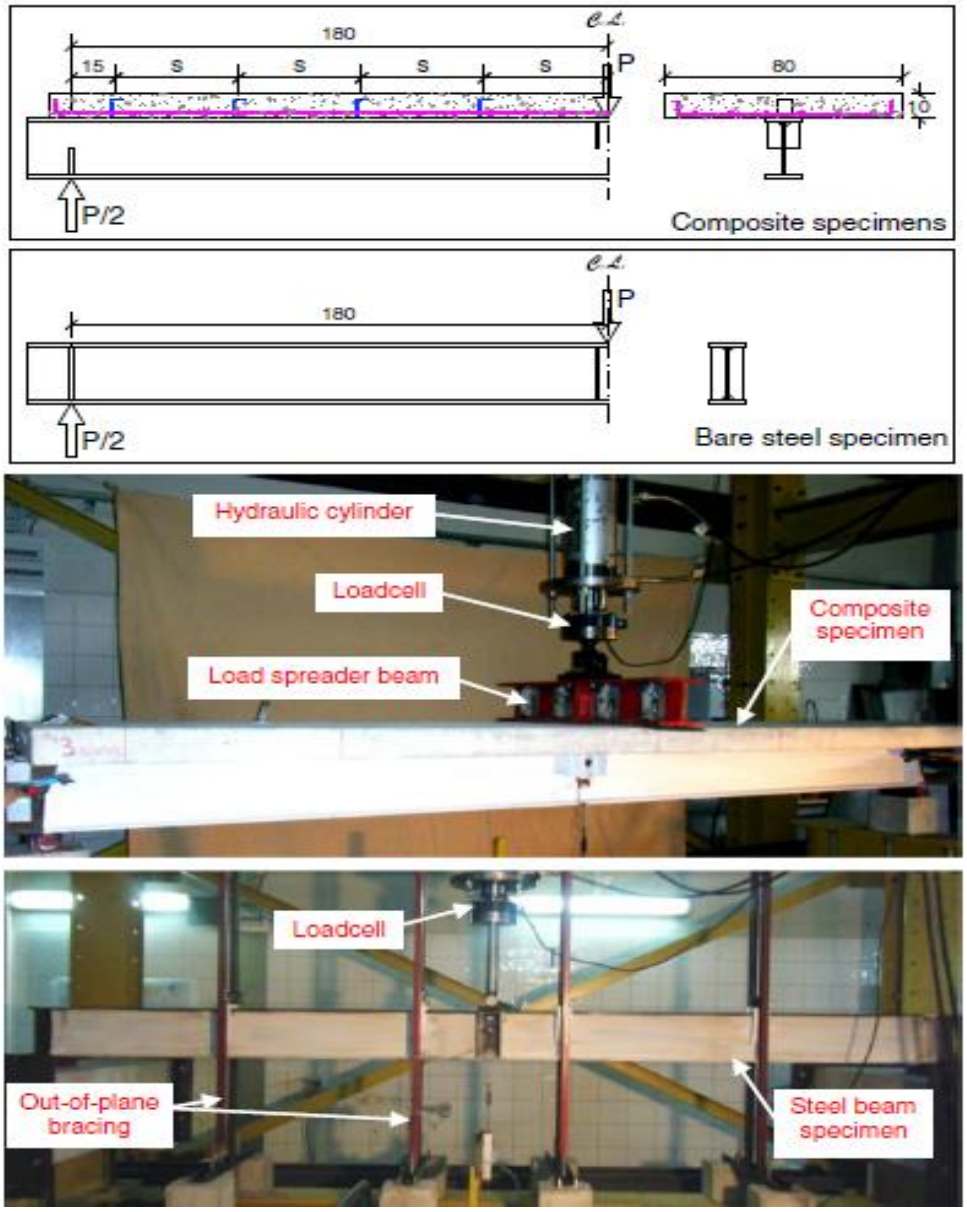

Figure 1.10. Details of specimen and setup for beam tests by Baran and Topkaya (2014)

1.5.1 Results of Pushout Tests

The failure mechanism observed in pushout specimens was the fracture of channel shear connector near the fillet between the web and the flange. Cracking on the sides of the concrete slab was also observed depending on the load level. Progression of the load led the cracking to the top surface of the concrete slabs. The

influence of channel length on the measured load capacity for different channel sizes is shown in Fig.1.11. Channel length and channel height are the two factors that have major influence on the loading capacity of a specimen. Increase in the channel length resulted an increase in the load capacity. For instance, UPN65x100 has 1.45 times loading capacity when compared with UPN65x50. The load capacity is also affected by the channel height. As the comparison of the load capacities belonging to UPN65x50 and UPN100x50 indicates, the effect of channel height is not as significant as the channel length. To give an example for UPN80 channel, as the channel length increased from 50 mm to 75 mm the loading capacity increased approximately 23% while further increasing it from 75 mm to 100 mm had only 6% increase in loading capacity and this decreasing trend of the rate of change was similar for all the specimens.

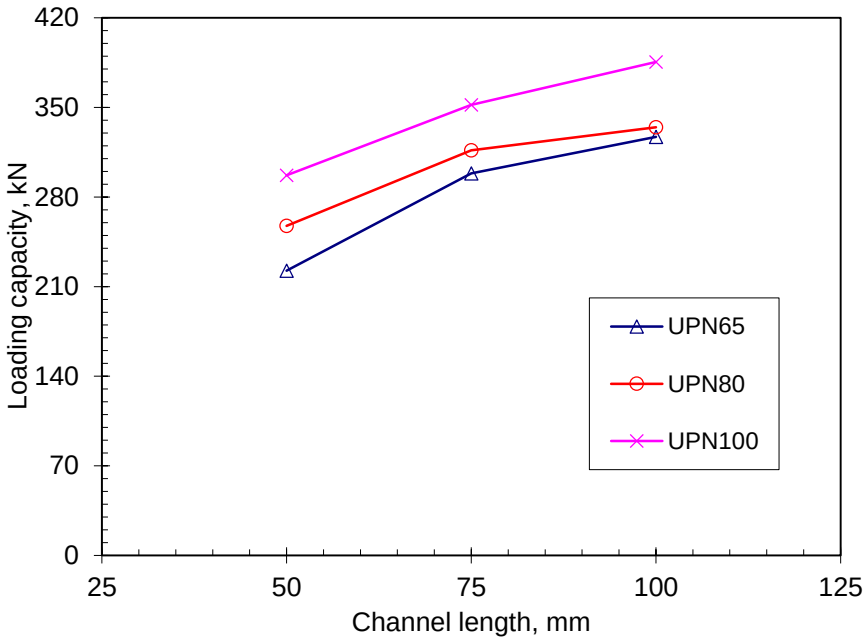

Figure 1.11. Variation of connector load capacity with channel length (Baran and Topkaya, 2012)

1.5.2 Results of Beam Tests

Load-deflection response of each beam specimen is presented in Fig. 1.12 in order to discuss the effect of the degree of composite action. As mentioned earlier, the lowest degree of composite action used in the specimens was 0.35 and three specimens

(6-UPN65x50, 5-UPN65x75 and 4-UPN65x100) had the degree of composite action larger than unity, i.e. these specimens had fully composite behavior. A degree of composite action as small as 0.35 resulted in a significant increase in stiffness and load capacity at service loads when compared to a bare steel beam tested without a concrete slab. Beam service stiffness and load capacity are observed to increase with the increasing degree of composite action.

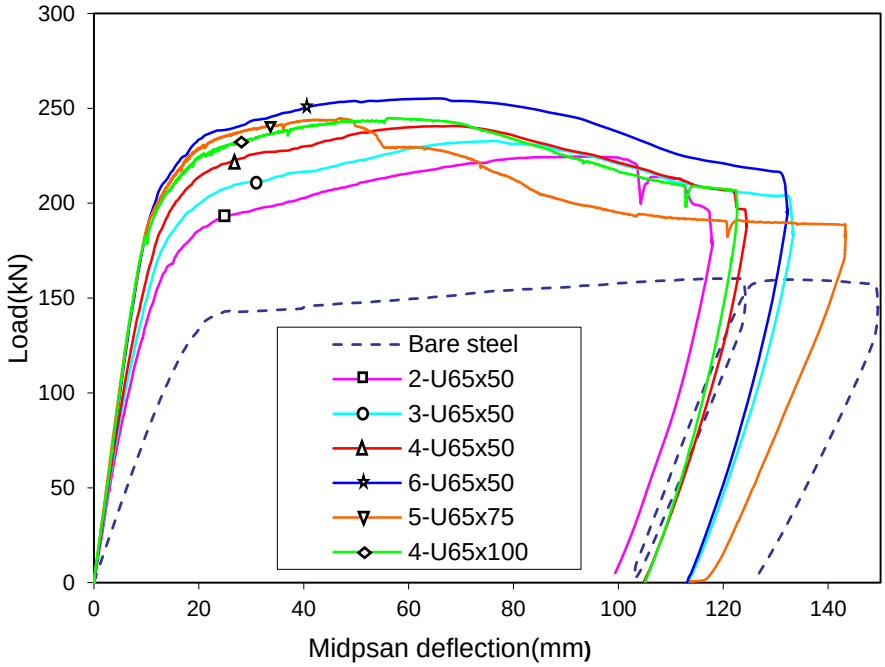

Figure 1.12. Load versus midspan deflection response of beam specimens (Baran and Topkaya, 2014)

1.6 ORGANIZATION OF THE THESIS

This thesis is divided into four chapters. Chapter 1 provides a general introduction to the basic mechanics of steel-concrete composite beams. A literature review on the use of various types of mechanical shear connectors, including channel type connectors, is presented. Previous experimental studies on pushout response of channel type shear connectors and on flexural behavior of steel-concrete composite beams utilizing this type of connectors is summarized.

Chapter 2 describes the numerical model used for the finite element analyses. Modeling details of the bare steel beam is explained first, followed by the description of composite beam models. Modeling of steel and concrete material response as well as the definition of the material parameters in the model used for the shear connectors are discussed in detail.

Results of the numerical analyses are explained in Chapter 3. Load-deflection response of composite beam models is presented and the stiffness and loading capacities are discussed in this part. The stiffness and loading capacity according to AISC (2010) was compared with the numerical and experimental results. Damage behavior of each time step, analysis of cross-sectional strain profile, slip behavior and verification of results with analytical solution, effect of shear connector location were also provided.

Chapter 4 presents a brief summary of the study and to the highlights of the conclusions reached.

CHAPTER 2

DESCRIPTION OF NUMERICAL MODEL

There are various formulations available in OpenSees framework. Among these formulations, the displacement-based beam-column elements were used to model the steel beam, the concrete slab, and the mild reinforcement in the current study. In this formulation, the beam displacements are estimated in terms of nodal values utilizing cubic Hermitian shape functions. The nonlinear curvature distribution was attained by defining multiple elements along the beam length. A distributed plasticity was assumed where the beam finite element is discretized into 2D fiber elements over the cross section at each integration point and a uniaxial stress-strain response is assigned to each fiber.

A displacement-controlled integrator was used such that the response of the composite beam was captured during the analysis for the given time step. For composite and bare steel beam models each time step used in the analysis corresponds to 0.2 mm transverse deflection at the beam centerline and the analyses were continued up to 75 mm midspan deflection.

2.1 OPENSEES FRAMEWORK

In this study two-dimensional fiber-based finite element models of full-scale composite beams utilizing nonlinear constitutive laws were developed within the OpenSees framework. OpenSees (Open System for Earthquake Engineering Simulation) framework is an open-source object oriented software framework allowing finite element applications for simulating response of structural and geotechnical systems (McKenna, 1997). In this framework there are predefined

material models available which, if needed, can also be extended by the user. The interpreter format is in Tcl language however the source code is primarily written in C++ using numerical libraries of Fortran or C for linear equation solving, material and element routines. The post-processing procedure is done using MATLAB, where each result is converted from text files to arrays. Throughout the modeling procedure used in the current study predefined displacement based beam-column elements were employed. A detailed description of the modeling techniques utilized is provided in the following part.

2.2 DESCRIPTION OF ELEMENTS AND FIBER MODELING

Fiber modeling is a valuable simulation technique since each fiber stores the material nonlinear data for each time step. By this mean, the stress and strain data could be pursued, the strain distribution in the transverse section could be followed and the slip between the concrete slab and steel beam could be obtained. A composite beam can be modeled in two alternative ways in OpenSees (Jiang et al, 2013). One is to use a single section including steel beam and concrete slab in order to represent the full composite action. The other method is to define steel beam and concrete slab separately as illustrated in Fig. 2.1. In the case where a complete composite action exists, i.e. no interface slip, between the concrete slab and steel beam, the finite element modeling can be achieved through a unified cross-section discretization containing the fibers of both the steel beam and the concrete slab. When the interface slip becomes significant, leading to a partially composite behavior, on the other hand, the steel beam and concrete slab have to be defined separately as independent finite elements with the shear connectors and constraints at the interface.

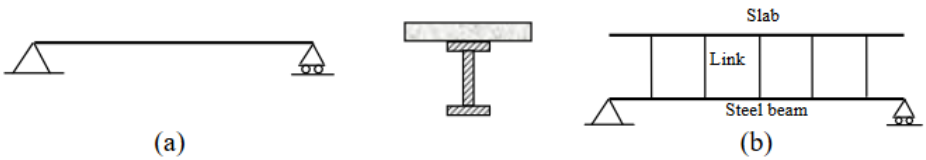

Figure 2.1. Schematic of OpenSees modeling approach (a) single section model; (b) rigid link model (Jiang et al., 2013)

In numerical models utilized in this study, two-dimensional elements belonging to the steel beam and the concrete slab were defined at their centroids. Nodes at the centroids of each material were connected to two different nodes sharing the same physical location. This location is where the steel beam and the concrete slab intersects. Steel beam and concrete slab cross sections had independent fiber discretization and the centroid of two cross sections did not coincide. The two nodes sharing the same physical location were then connected to each other with a *zeroLength* element available in OpenSees, as illustrated in Fig. 2.2. Rigid link elements were defined between the nodes that were connected to each other with these *zeroLength* elements. The *zeroLength* elements defined at beam-slab interface were assigned *Pinching4* material for inelastic response in the horizontal direction, while the vertical displacements and rotations of the steel beam and concrete slab were constrained using *EqualDOF* command of OpenSees.

A modeling approach similar to the one explained above was adopted for the numerical model used to study fully composite response, except that the interface nodes at the element ends sharing the same physical location were constrained using *EqualDOF* command to have the same horizontal and vertical displacements, as well as rotation. This way a “no-slip case” was obtained at steel-concrete interface.

In the tests done by Baran and Topkaya (2014) the steel beams were made of IPE240 section, which has 240 mm total depth, 120 mm flange width, 6.2 mm web thickness and 9.8 mm flange thickness. The concrete slab had 800 mm width and 100 mm thickness. The fiber sections used in the numerical models created as part of this study also match these dimensions.

For all of the numerical models, the total length of the beam was 3600 mm, and this length was divided into 72 finite elements each having 50 mm length. Fiber discretization of steel beam was based on 4 horizontal and 16 vertical fibers for flanges and 4 vertical and 16 horizontal fibers for the web, as indicated in Fig. 2.2. The concrete slab was divided into 32 fibers both in the vertical and horizontal directions. A relatively fine fiber discretization was used for the slab both for convergence purposes and also to capture the spread of inelasticity over the entire length and width of the slab accurately. The mild steel reinforcing bars embedded inside the concrete

slab near the bottom surface were added in the fiber section using *layer* command of OpenSees. Bar spacing was 120 mm as in the tests, therefore 6 bars of 10 mm diameter were introduced to the bottom of the concrete slab. The clear cover was defined as 25 mm from bottom and sides of the concrete section.

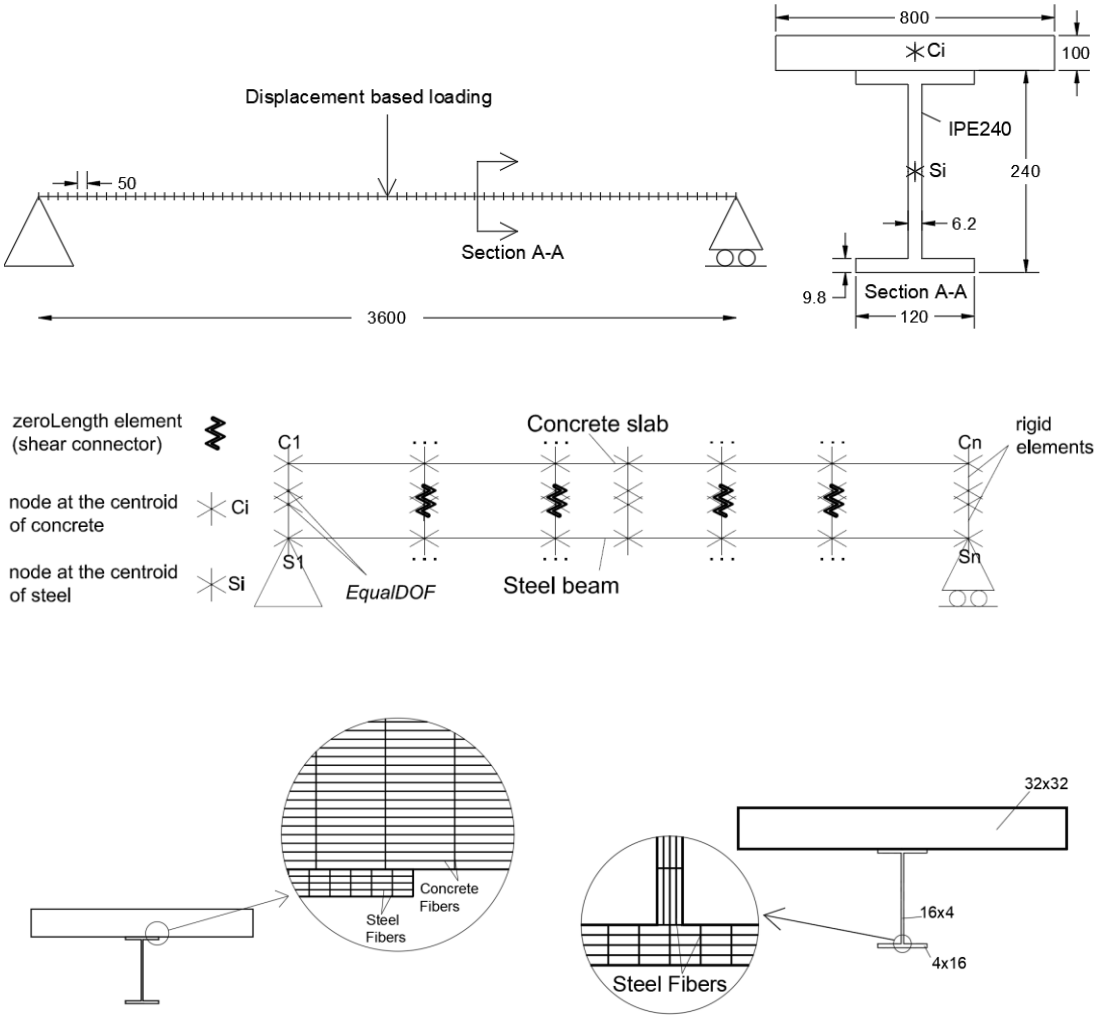

Figure 2.2. Schematic definition of geometry and and fiber modeling of the numerical models

For numerical models, there were six different composite beam models with different degree of composite action and a bare steel model. The number and location of shear connectors in each shear span were same as the beam specimens tested by Baran and Topkaya (2014). Table 2.1 shows the information regarding the shear connectors used in each model and the corresponding degree of composite action.

Models 6-UPN65x50, 5-UPN65x75 and 4-UPN65x100 are the full composite models according to AISC Specification (2010), whereas models 2-UPN65x50, 3-UPN65x50 and 4-UPN65x50 are the partially composite models with the degree of composite action varying between 0.35 and 0.70.

Table 2.1. Properties of beam models

Beam model name	**Number of shear connectors per shear span**	**Shear Connector Length, mm**	**ΣQn/FyAs**
Bare Steel	-	-	-
2-UPN65x50	2	50	0.35
3-UPN65x50	3	50	0.53
4-UPN65x50	4	50	0.70
6-UPN65x50	6	50	1.06
4-UPN65x100	4	100	1.04
5-UPN65x75	5	75	1.19

2.3 DEFINITION OF MATERIAL PARAMETERS USED IN NUMERICAL MODELS

2.3.1 Modeling of Steel Material Behavior

In order to represent a bare steel beam, numerical model of a steel beam made of IPE240 cross section with no concrete slab was created. The uniaxial stress-strain response used for the steel material was based on *Steel4* material developed by Zsaróczay (2013), which was developed as an extension of Giuffré-Menegetto-Pinto model including both the isotropic and kinematic hardening properties, as well as the ultimate strength limit. The steel yield strength for the beams tested by Baran and Topkaya (2014) was measured to be 315 MPa for the web and 365 MPa for the flanges.

Based on these measured values, the bare steel model was analyzed twice using the steel strength values of 315 and 365 MPa. For both cases the ultimate strength was taken as 466 MPa (Table 2.2).

The steel stress-strain behavior obtained by Baran and Topkaya (2014) from coupon tests and the one utilized in the numerical models used in this study are shown in Fig. 2.3. The parameters used to define the steel material models are tabulated in Table 2.2 and Fig. 2.4 shows what are the meaning of these parameters on stress-deformation plots noting that the values are just as they were in the OpenSees Manual. As mentioned in Chapter 3 of the thesis, using a steel yield strength of 315 MPa for the bare steel beam provides a good match between the numerically determined and experimentally obtained load-deflection response. Therefore, this steel yield strength value was used in composite beam models.

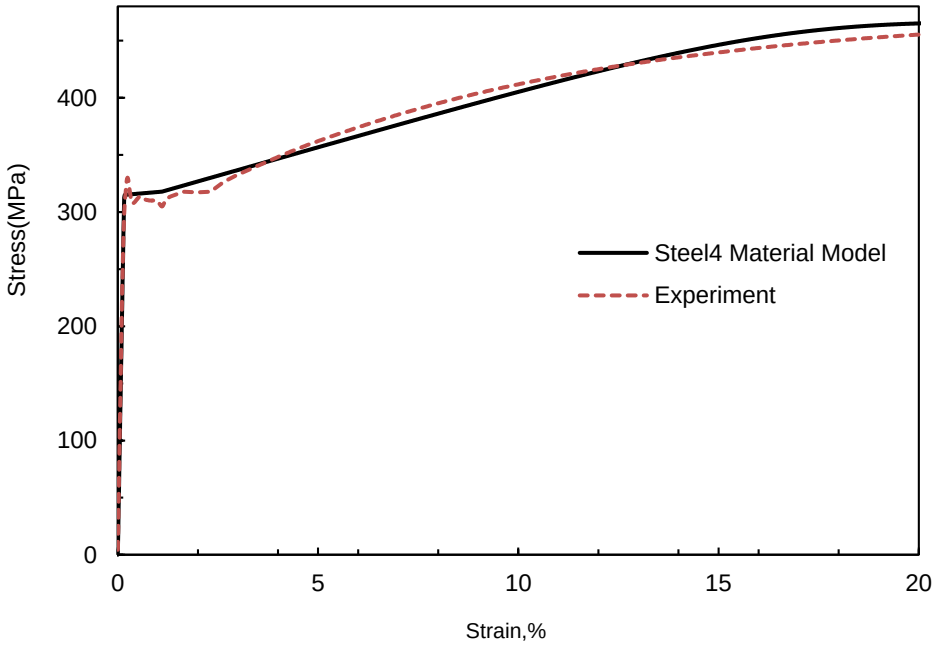

Figure 2.3. Stress-strain behavior steel used in specimens and in *Steel4* material model respectively

Table 2.2. *Steel4* material properties for B1 and B2 steel model

Name of the Steel Model	**B1**	**B2**
Yield strength, f_y	315 MPa	365 MPa
Ultimate strength, f_u	466 MPa	466 MPa
Modulus of elasticity, E_0	200 GPa	200 GPa
Kinematic hardening ratio, b	0.15%	0.15%
Radius of kinematic hardening, R_0	50	50
Exponential translation parameters r1 and r2	0.91 and 0.15	0.91 and 0.15
Initial isotropic hardening ratio, b_i	0.35%	0.35%
Saturated isotropic hardening ratio, b_I	0.08%	0.08%
Position of intersection point between initial and saturated hardening asymptotes, ρ_i	1.30	1.39
Transition radius, R_i	25	25
Length of the yield plateau, I_p	6	6
Exponential transition from kinematic hardening to perfectly plastic asymptote, R_u	2	2

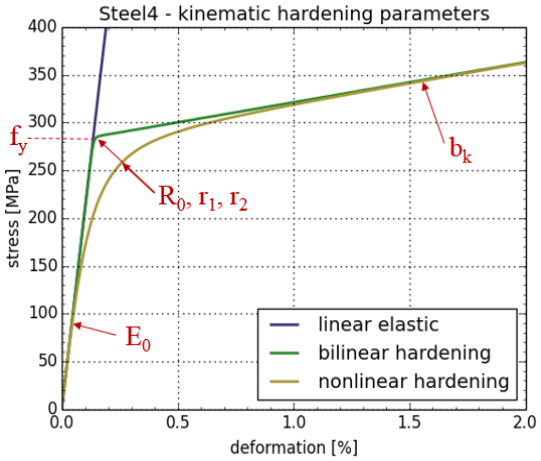

(a)

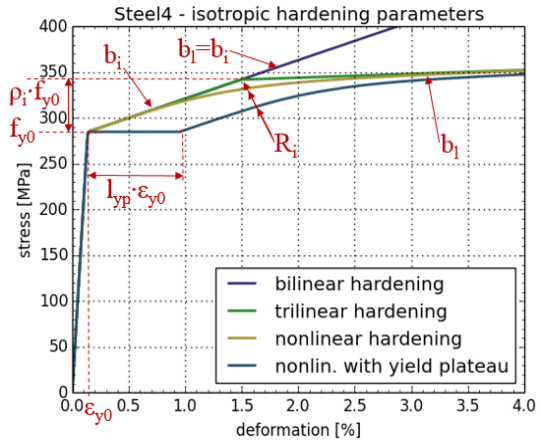

(b)

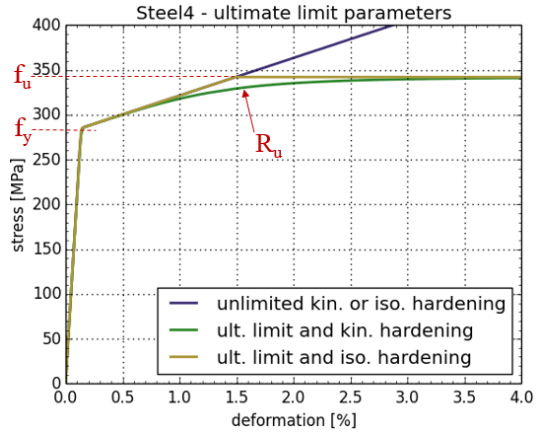

(c)

Figure 2.4. *Steel4* material parameters (a) kinematic hardening (b) isotropic hardening (c) ultimate limit (OpenSees Command Manual, 2012)

2.3.2 Modeling of Shear Connector Response

Shear connector load-slip response was retrieved from the pushout tests done by Baran and Topkaya (2012). *Pinching4* material available in OpenSees was implemented to model channel shear connectors accounting for yielding, strength and stiffness degradation, and softening. OpenSees *Pinching4* material model has four floating points for force and deformation both on the positive and negative response envelope as shown in Fig. 2.5.

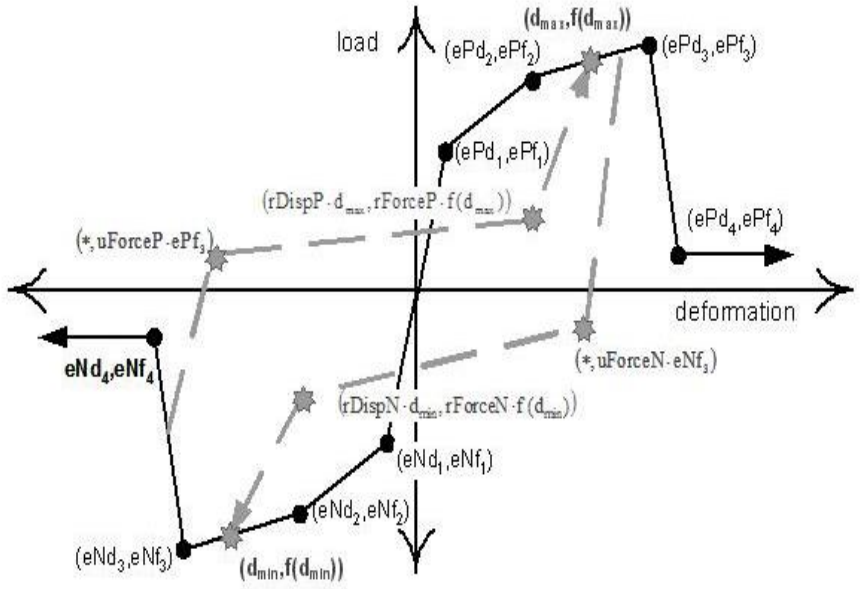

Figure 2.5. Load deformation input values for *Pinching4* material model (OpenSees Command Manual, 2012)

As shown in Fig. 2.6 and tabulated in Table 2.3, the required parameters for *Pinching4* material model were determined for each channel connector considering the experimentally determined load-slip response from the pushout test specimens tested by Baran and Topkaya (2012). As evident in the figure, pushout response of channel shear connectors does not exhibit strength and stiffness degradation or softening. Therefore, it may be argued that the connector modeling could be achieved by using a simpler material model than *Pinching4*. However, *Pinching4* material model was chosen in analyses based on its nonlinear capability and numerically stable behavior that it offers.

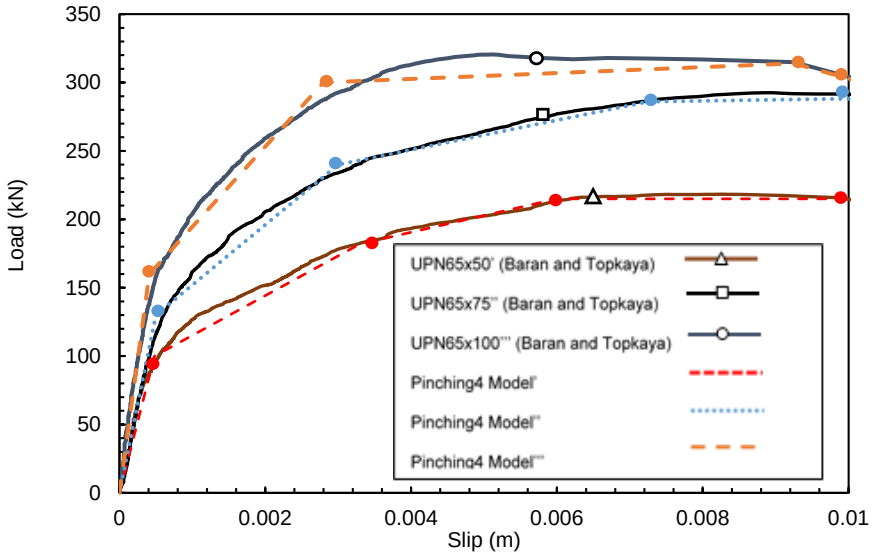

Figure 2.6. Channel connector pushout test results and *Pinching4* material model

Table 2.3. *Pinching4* Material Properties for UPN65x50, UPN65x75 and UPN65x100 connector models

Load(kN), Deformation(mm)	UPN65x50	UPN65x75	UPN65x100
ePf1, ePd1	100, 0.48	130, 0.50	160, 0.41
ePf2, ePd2	182, 3.30	240, 3.00	300, 2.80
ePf3, ePd3	215, 6.00	286, 7.25	314, 9.25
ePf4, ePd4	215, 11.00	289, 11.00	278, 11.00

2.3.3 Modeling of Concrete Material Behavior

Determination of material properties of concrete was one of the most challenging part of the modeling study. Convergence issues were faced with during analyses especially due to early cracking of concrete. *Concrete02* material model was used in order to achieve a relatively easy converging response, since the tensile cracking behavior could be defined by specifying a very low tensile softening stiffness in this material model. The compressive strength of *Concrete02* material was specified as 32 MPa. Tensile cracking in concrete was considered by specifying cracking

strength and softening stiffness. The input data necessary to define the *Concrete02* material model is illustrated in Fig. 2.7. Modulus of elasticity of concrete was taken as 32000 MPa. Concrete tensile strength value was specified as 1.98 MPa based on linear interpolation of concrete class and mechanical properties table of TS 500 (2000). The other parameters used to define the concrete material model are tabulated in Table 2.4. Although unconfined concrete model is more suitable for the concrete slab. Due to convergence problems regarding the crushing of concrete, strain at crushing strength was used to be a slightly higher value of 0.025.

Table 2.4. *Concrete02* material properties

***Concrete02* Parameters**	**Material Properties**
Concrete compressive strength, fpc	32 MPa
Concrete strain at maximum strength, epsc0	0.002
Concrete crushing strength, fpcu	3.2 MPa
Concrete strain at crushing strength, epsU	0.025
Ratio between unloading slope at epscu and initial slope, lambda	0.125
Tensile strength	1.98 MPa
Tension softening stiffness	10^{-6}

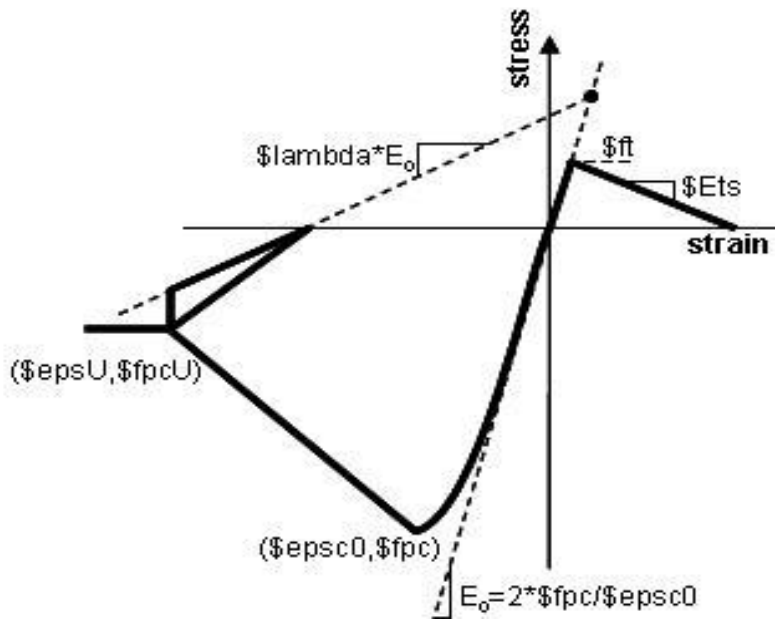

Figure 2.7. Stress strain response for *Concrete02* material model

2.3.4 Modeling of Mild Reinforcement Response

Mild reinforcement was embedded in the fiber section using *layer* command which differentiates from other fiber section materials such as concrete and steel. Using this command OpenSees allows user to define longitudinal reinforcement by simply specifying the number of bars and the area of each bar. The total number of longitudinal bars were six and each were 10 mm diatemer bars as in the tests. Transverse bars used in the test were not defined since these were reinforcement for assembly purposes. The material model used for the reinforcement is *Steel01* uniaxial bilinear steel material with kinematic hardening. No kinematic hardening was used due to the lack of tensile test data for the reinforcement, for simplicity, elastic perfectly plastic steel model was used. The stress-strain behavior for material constitutive relation is shown in Fig. 2.8 and the material properties are given in Table 2.5. Analyses indicated that the mild reinforcement does not have a significant impact on the overall behavior of composite beams. However, in one of the models (model 5-UPN65x75) serious convergence problem was encountered due to rapid crushing of concrete. As a remedy additional reinforcement with a very small area (10^{-2} times smaller compared to bottom reinforcement) and significantly high yield strength (10^{6}

times larger than the value specified in Table 2.5) was placed near the top of the concrete slab. It should be noted that placing such additional reinforcement near the top of concrete slab should not cause a major influence on the overall beam response under positive moment.

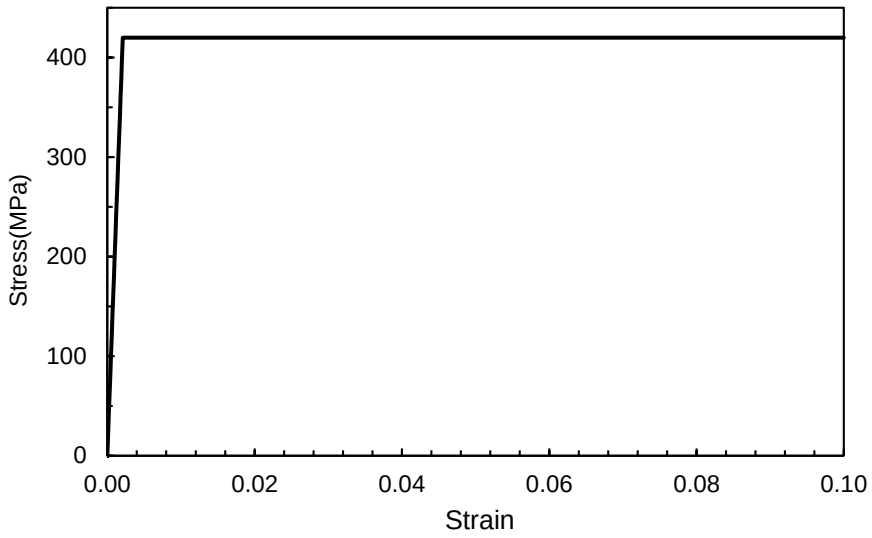

Figure 2.8. Stress strain response for *Steel01* material

Table 2.5. Steel01 material properties

***Steel01* Parameters**	**Material Properties**
Yield strength, Fy	420 MPa
Initial elastic strength, E0	200 GPa
Strain hardening ratio, b	0

CHAPTER 3

RESULTS OF NUMERICAL MODELS

3.1 BEAM LOAD CAPACITY

Results of the numerical analyses are compared with the experimentally determined response in terms of beam stiffness and load capacity. The comparison is provided first for the bare steel beam analyzed with no concrete slab, followed by composite beams. The load versus midspan deflection behavior of the bare test beam is given in Fig. 3.1 together with the predicted response. As explained earlier, the bare steel model was analyzed with two different steel yield strengths of 315 and 365 MPa. As evident in the plots presented in Fig. 3.1, both steel strengths resulted in accurate prediction of the experimentally determined stiffness of the test beam. In terms of load capacity and the overall load-deflection response, however, the model with 365 MPa steel strength provides a better agreement with the measured response than 315 MPa strength.

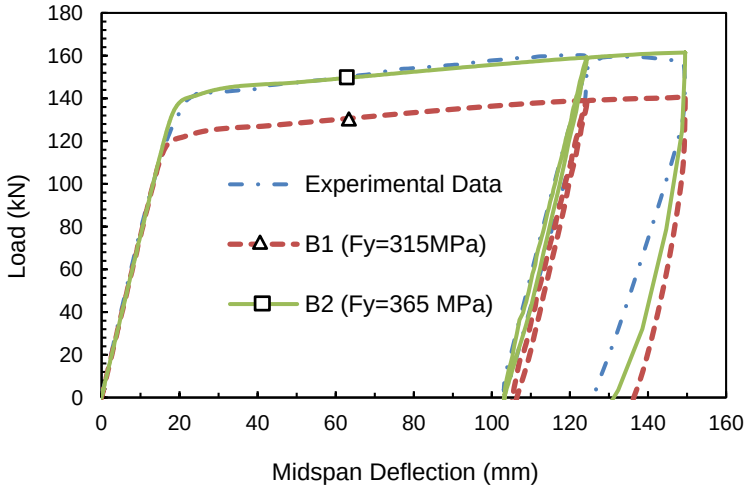

Figure 3.1. Load versus midspan deflection response for bare steel beam

Numerically determined load-deflection response of each composite beam is given in Fig. 3.3 together with the measured response from experiments. Close agreement between the numerically determined and experimentally obtained response over the entire range of load-deflection curves is evident for these beams, irrespective of the degree of composite action present. Such a close match is an indication of the accuracy of material models used for the steel, concrete, as well as the shear connectors in the numerical models.

Superimposed on the plots in Fig. 3.3 is the computed load capacity of beams based on a simple procedure utilizing rectangular compressive stress block for concrete and elasto-plastic stress-strain behavior for steel. An example illustration for this type calculation is given in Fig. 3.2. The concrete force is calculated as $0.85f_cA_c$ rectangular stress block assumption and steel force as f_yA_s. The location of neutral axis is identified from equilibrium equations. The moment of the internal force couple is then calculated. The loading capacity is determined afterwards simply since moment is PL/4 for simply supported beam with concentrated loading. As evident on the plots, the load capacity from the simple code procedure generally predicts the beam capacity with acceptable accuracy. The load capacity determined this way underestimates the capacity of partially composite beams (models 2-UPN65X50, 3-UPN65X50, and 4-UPN65X50), while the load capacity of fully composite beams (models 4-UPN65X100, 5-UPN65X75 and 6-UPN65X50) is slightly overestimated.

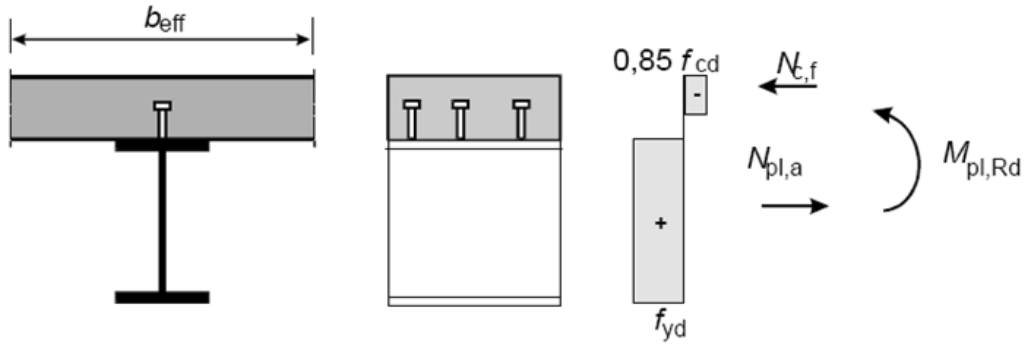

Figure 3.2. Internal force couple used in calculation of moment capacity (Retrieved from steelconstrucion.info)

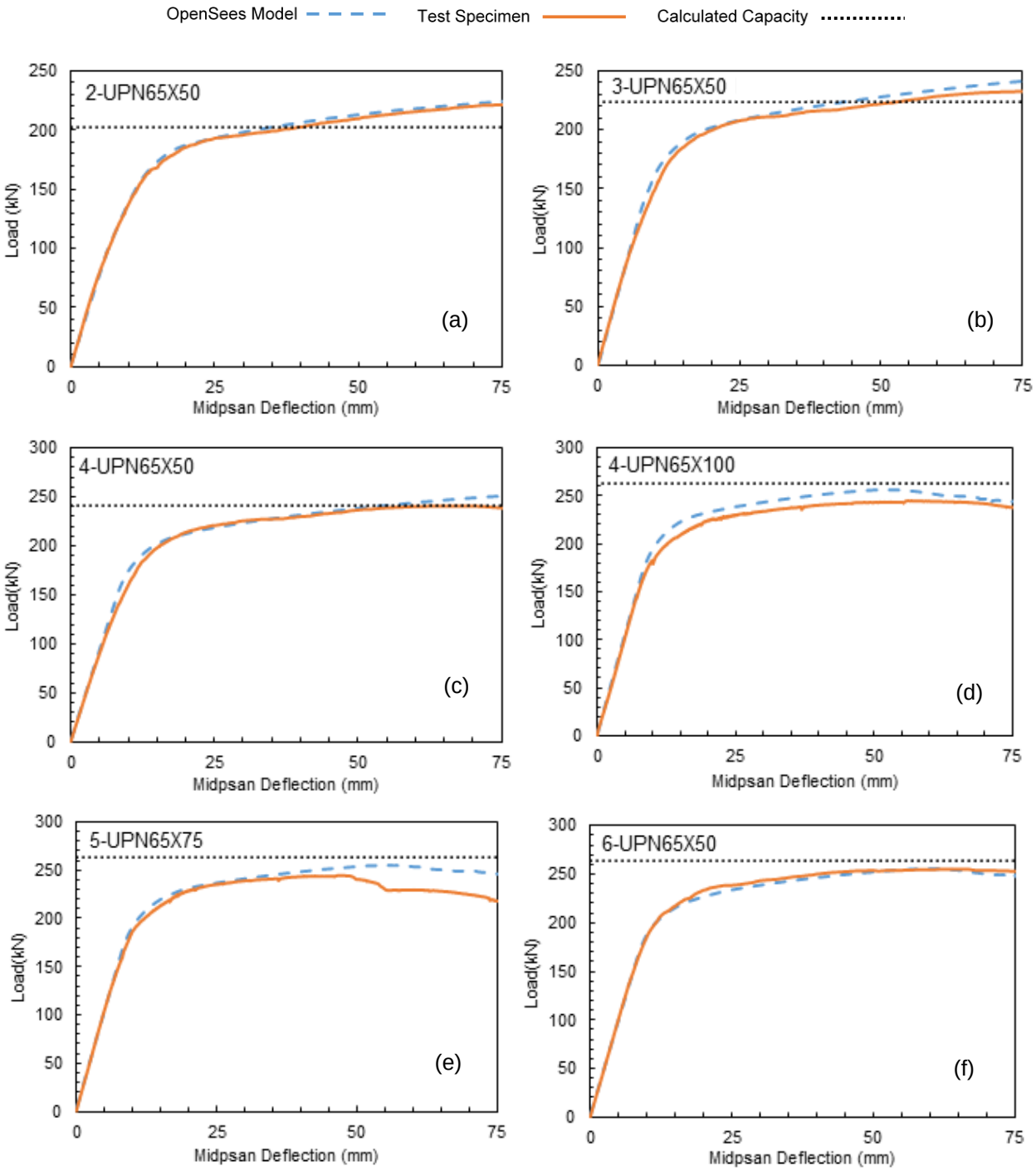

Figure 3.3. Load versus midspan deflection response of composite beams

Based on the AISC (2010) definition, these are the beams with a $\sum Q_n/F_yA_s$ (degree of composite action) value larger than unity: 4-UPN65X100, 5-UPN65X75 and 6-UPN65X50. Even though these three beams are expected to have a fully composite behavior as their $\sum Q_n/F_yA_s$ value is larger than unity, they fail to reach the stiffness and load capacity of the full composite constrained model. The reason for such a response is the fact that even though the interface connectors in these beams provide horizontal shear force capacity exceeding the crushing capacity of concrete slab or yielding capacity of steel beam, there is still a nonzero interface slip. Such interface slip, even it is a small amount, violates the fully composite response and results in reduced stiffness and load capacity, as shown in Fig. 3.4. In order to investigate the fully composite beam response, in one of the numerical models the bottom surface of concrete slab and the top surface of steel beam were constrained to have the same longitudinal displacement. This way, no relative slip is allowed between the concrete slab and the steel beam at the interface.

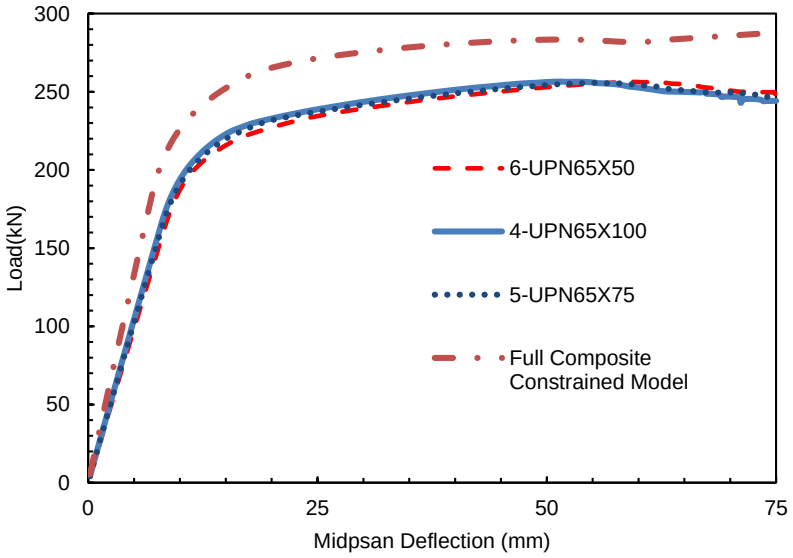

Figure 3.4. Comparison of measured and predicted fully composite response

It should be mentioned here that a cross-sectional analysis of the composite beam section utilizing an equivalent rectangular stress block for concrete and an elasto-plastic stress-strain relation for steel resulted in a load capacity of 263 kN. When the concrete rectangular stress block is replaced with a more realistic nonlinear stress-strain behavior the load capacity increases to 274 kN. Finally, including the strain

hardening response of steel increases the load capacity of the composite beam section to 299 kN. A summary of these calculated values is provided in Table 3.1. The load capacity calculation for nonlinear distribution was done by integrating stress distribution times the layer area throughout the height of the composite section and finding the location of plastic neutral axis. After determination of plastic neutral axis, moment is taken by integrating moment arm times the stress distribution for each layer area. The schematic representation of each load capacity calculation is given in Fig. 3.5.

Table 3.1. Load capacities of the full composite section

Steel Model	**Concrete Model**	**Calculated Load Capacity (kN)**
Perfectly plastic	Rectangular stress block	263 (a)
Perfectly plastic	Non-linear	274 (b)
Strain hardening	Non-linear	299 (c)

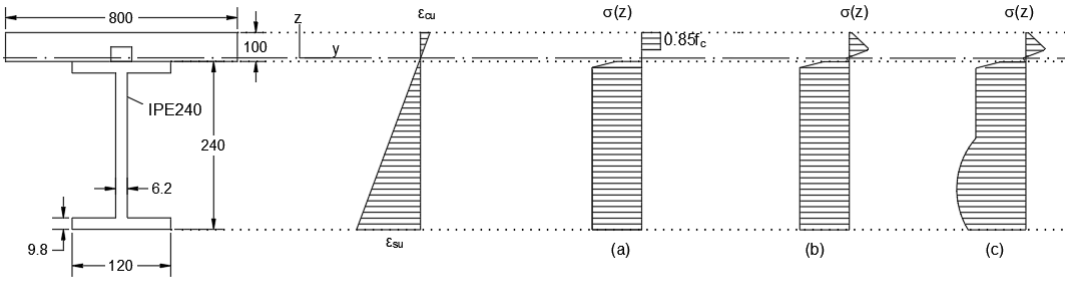

Figure 3.5. Stress distribution for calculation of the loading capacity

3.2 BEAM STIFFNESS

The American Institute of Steel Construction Specification for Structural Steel Buildings (AIS3-UPN65X5060-10) provides methods for calculating the elastic stiffness of the partially composite beams. The effective moment inertia can be approximated by :

$$I_{eff} = I_s + \sqrt{\frac{\sum Q_n}{C_f}}.(I_{tr} - I_s) \qquad \text{(Eq. 3.1)}$$

where I_s is the moment of inertia of steel beam, I_{tr} is the moment of inertia of full composite uncracked cross-section, and C_f is the minimum compressive force in the full composite beam, namely the minimum of $A_s x F_y$ and $0.85 x f'_c x A_c$. The depth of concrete slab under compression depends on the degree of partial composite action. For fully composite sections the location of the neutral axis depends on whether the tensile strength of steel section exceeds the compressive strength of concrete section or not. For partially composite beams, however, the net compressive force on the concrete slab is determined by the summation of the force capacity of the connectors $\sum Q_n$ in between the point of zero moment and maximum moment. Depth of the compressive part of the concrete slab can be determined using the expression in :

$$a = \frac{\min(A_s F_y, 0.85 f'_c A_c, \sum Q_n)}{0.85 f'_c b} \qquad \text{(Eq. 3.2)}$$

Noting that using linear elastic theory in calculation of the effective moment of inertia overestimates the stiffness of the composite beams, the AISC Specification (2010) recommends to reduce I_{eff} by 25%.

An alternative method is provided in the Commentary to the AISC Specification (2010) to determine a lower bound moment of inertia, I_{LB} to be used in deflection calculations. As illustrated in Fig. 3.6, the concrete deck in this method is replaced by an equivalent steel area based on the ratio of compressive strength of the concrete to the yield strength of the steel. I_{LB} can be calculated according to Equation

3.3. In this equation, A_s is the cross-sectional area of the steel section, Y_{ENA} is the distance from the bottom of the beam to the elastic neutral axis, which can be determined using Equation 3.4, d is the depth of the beam, and Y_2 is the distance from the internal compressive force on concrete to the beam top flange, which can be determined using Equation 3.5.

$$I_{LB} = I_s + A_s(Y_{ENA} - \frac{d}{s})^2 + \frac{\sum Q_n}{F_y}.(d + Y_2 - Y_{ENA})^2 \quad \text{(Eq. 3.3)}$$

$$Y_{ENA} = \frac{\left[\frac{A_s d}{2} + \left(\frac{\sum Q_n}{F_y}\right)(d + Y_2)\right]}{[A_s + (\frac{\sum Q_n}{F_y})]} \quad \text{(Eq. 3.4)}$$

$$Y_2 = Y_{con} - \frac{a}{2} \quad \text{(Eq. 3.5)}$$

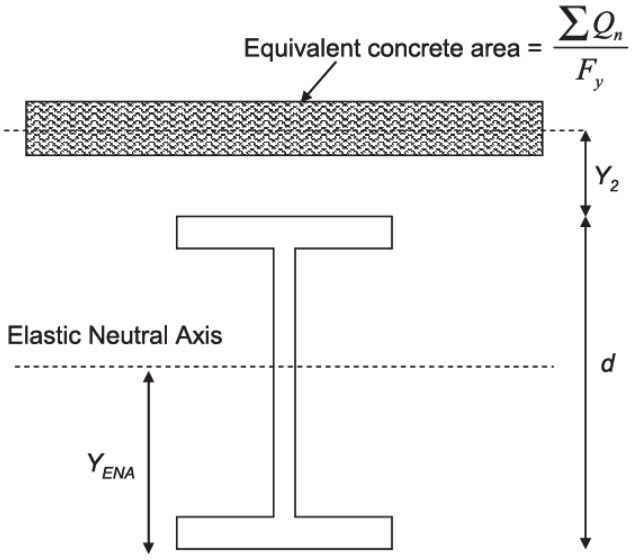

Figure 3.6. Effective cross section for lower bound moment of inertia calculations (Baran and Topkaya, 2014)

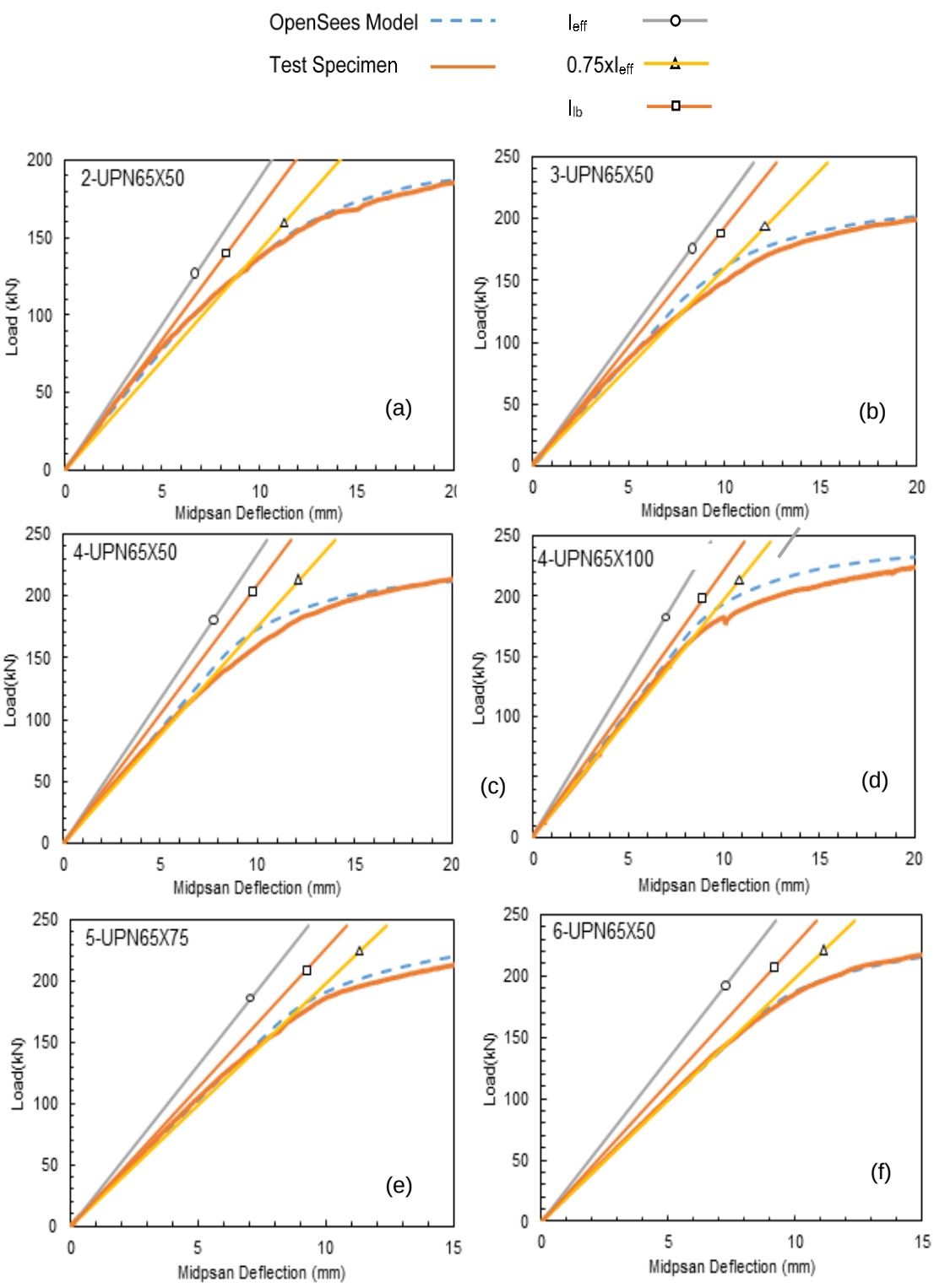

Figure 3.7. Relation between predicted stifnesses and load-deflection response

It should be noted that, according to Commentary to the AISC Specification (2010) plastic distribution of the forces is neglected for flanges under compression. Therefore lower bound moment of inertia for a section differentiates between factored ultimate load and service load. I_{LB} under service load is higher than the factored ultimate load I_{LB}. Therefore, I_{LB} should be used in deflection calculations specifically.

The relation between the beam stiffness obtained using three different moment of inertia values, namely I_{eff}, $0.75xI_{eff}$ and I_{LB}, and the numerically predicted load-deflection response is presented in Fig. 3.7. Using I_{eff} and I_{LB} results in overestimation of the beam stiffness for all degrees of composite action studied. On the other hand, reducing the effective moment of inertia by 25%, as suggested by the AISC Specification, matches the numerically obtained elastic beam stiffness fairly well.

3.3 DAMAGE BEHAVIOR

Damage behavior is another interesting outcome that could be observed by using the results obtained from the fiber models. In order to do this, the stress and strain condition for each fiber was recorded during analysis at 0.2 mm transverse midspan deflection increments. Extent of damage on steel beam and concrete slab were plotted in Fig. 3.8. These plots depict the progression of damage under increasing load and allows the investigation of how the influence of different types of damage is reflected on the overall deflection response of the composite beams. The four damage types plotted in the figure are: (1) tension yielding of the steel beam, (2) compression yielding of steel beam, (3) cracking of concrete slab, and (4) crushing of concrete slab. The percent damage values shown in the plots represent the number of beam or slab fibers that underwent the indicated damage type normalized by the total number of beam or slab fibers. As seen in the plots, concrete cracking in slab starts to occur at very early stages of loading and progresses very quickly irrespective of the degree of composite action. The initiation and progression of concrete cracking do not cause a major influence on the load-deflection response of beams.

Concrete cracking was followed by the initiation of tension yielding at the bottom part of steel beam. It can be seen that as the degree of the composite action

increases the steel beam yielding initiates at slightly smaller midspan deflection values. This is attributed to the higher flexural stiffness of beams with high degree of composite action. With the progression of loading, approximately 65% of steel beam fibers yields in tension in Model 2-UPN65X50, which has the smallest degree of composite action. The beam yielding in models with full composite action (4-UPN65X100, 5-UPN65X75, and 6-UPN65X50) was observed to be more extensive with the ratio of steel beam fibers yielding in tension being approximately 80%. The extent of yielding in compression part of steel beam, on the other hand, is higher in models with smaller degree of composite action. This was an expected result, considering that as the strength and stiffness of shear connectors in the interface increase the compression demand on steel beam decreases and that on concrete slab increases.

Damage charts provided in Fig.3.8 also indicate that crushing of concrete slab occurred to some extent in fully composite models (4-UPN65X100, 5-UPN65X75, and 6-UPN65X50) at a midspan deflection of 75 mm. No concrete crushing was observed up to this midspan deflection level in other models, where the degree of composite action is smaller than unity. Again, this observation indicates the higher compression demand on concrete slab in models with high degree of composite action.

In order to investigate the damage behavior in a more consistent manner, two points, indicating the yielding of entire bottom flange and top flange, were indicated on the load-deflection plot for each model in Fig. 3.8. As evident in the plots, the entire bottom flange yielding occurs immediately after the initiation of yielding at bottom surface of steel beam. For all six models investigated, the point that the initial portion of the load-displacement curve deviates from linear response coincides with the point indicating the yielding of the entire bottom flange of steel beam. Therefore, based on the numerical results it can be concluded that linear load-deflection behavior continues until the full yielding of beam bottom flange, rather than the initiation of yielding as it would be expected. Yielding of beam top flange in compression occurs only in models with relatively low degree of composite action and this deformation mode disappears as the degree of composite action increases.

Material damage in terms of tension yielding of steel beam and cracking of concrete slab in each model is determined at midspan deflection values of L/360, L/300, and L/240. These deflection values cover the serviceability limits imposed on composite beams by various design specifications. The results are presented in Table 3.2. As mentioned earlier, the extent of steel beam yielding in tension increases with the increasing degree of composite action. For example, at the deflection limit of L/360, the ratio of steel beam fibers undergoing tension yielding is zero, 0.04, and 0.21, respectively for composite action levels of 0.35, 0.53, and 0.70. For beams with the composite action level greater than unity, the ratio of beam fibers undergoing tension yielding stays almost constant at approximately 0.3. Structural design approaches adopted in modern design codes ensure that the material remains elastic at service conditions. The yielding ratios shown in Table 3.2 may seem to contradict with this philosophy. However, the results indicate that for beams with relatively small degree of composite action the stiffness is relatively small and the design is controlled by the serviceability requirement. As the degree of composite action increases, the beam gets stiffer and as a result the serviceability requirement is automatically satisfied. For these beams, the design is controlled by the strength requirement.

Table 3.2. Ratio of beam fibers undergoing tension yielding at different serviceability limits

Beam	L/360	L/300	L/240
2-UPN65X50	0.00	0.17	0.38
3-UPN65X50	0.04	0.29	0.46
4-UPN65X50	0.21	0.38	0.50
6-UPN65X50	0.29	0.46	0.58
4-UPN65X100	0.33	0.50	0.63
5-UPN65X75	0.33	0.50	0.63

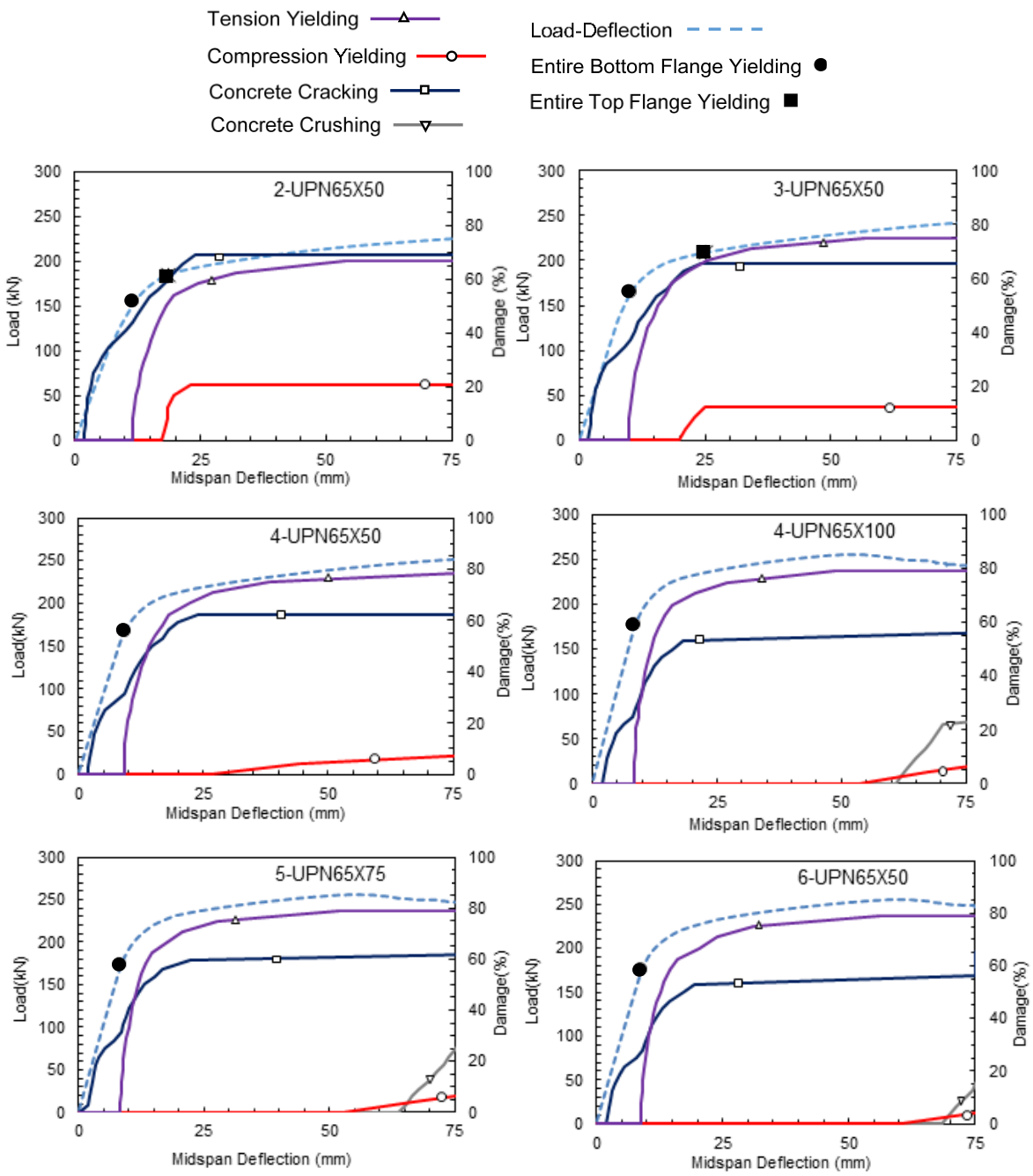

Figure 3.8. Damage response of the fibers

3.4 ANALYSIS OF CROSS-SECTIONAL STRAIN PROFILE

Variation of strain distribution at midspan section of models 2-UPN65X50 and 5-UPN55X75, which are respectively the models with the smallest and the largest

degree of composite action, is given in Fig. 3.9. The partially composite behavior in model 2-UPN65X50 reveals itself in the form of discontinuous strain profiles. In the case where no composite action exists between the steel beam and the concrete slab, i.e., no horizontal shear force transfer at the interface, the neutral axis would be located at the midheights of the steel beam and the concrete slab. As a result of the 35% composite action available in model 2-UPN65X50, the neutral axis in the steel beam is located at approximately 140 mm from the bottom surface, as opposed to 120 mm that would be expected when there is no composite action. Because the degree of composite action in model 5-UPN55X75 is larger than unity, theoretically a continuous strain profile across the interface would be expected. However, as evident in Fig. 3.9, there is a difference in the strains at the top surface of the steel beam and the bottom surface of the concrete slab, indicating a nonzero slip between the concrete slab and the steel beam at the interface. Such a lack of strain compatibility is an indication that even the total horizontal shear force capacity of connectors provided at the interface is sufficient to develop full yielding of the steel beam or crushing of the concrete slab, this condition does not guarantee a no-slip case and hence a continuous strain profile. The magnitude of interface slip and the extent of strain compatibility between the concrete slab and the steel beam are dictated by the stiffness of the shear connectors.

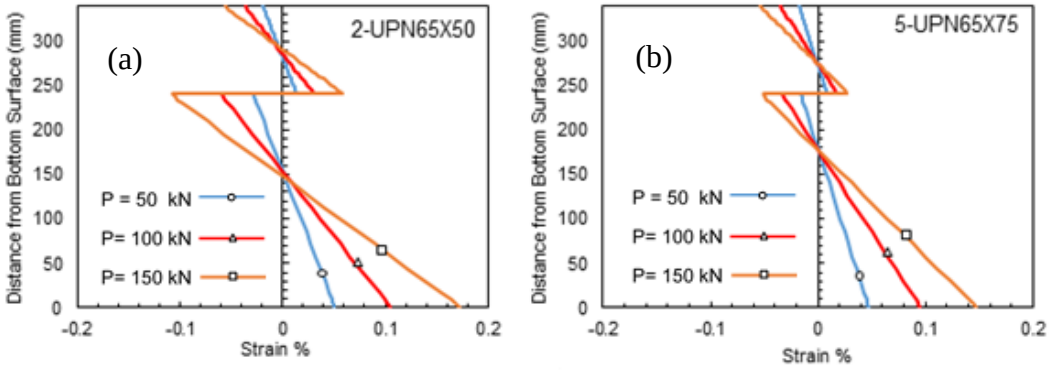

Figure 3.9. Strain profile of models with the smallest (a) and largest (b) degree of composite action

3.5 INTERFACE SLIP BEHAVIOR AND VERIFICATION WITH ANALYTICAL SOLUTION

Influence of the degree of composite action on the magnitude of relative interface slip between the concrete slab and the steel beam is depicted in Fig. 3.10. Each curve represents the variation of interface slip along the beam half-length at a midspan deflection of 75 mm. Because a concentrated load is applied at beam midspan, the interface slip increases rapidly starting from the midspan section and reaches to an almost constant value after a certain distance. For example, for model 2-UPN65X50, which had the lowest degree of composite action, 90% of the total interface slip measured at beam end occurred within approximately 0.50 m from the midspan section. For model 5-UPN65X75, with the largest degree of composite action, 0.15 m distance is required for the interface slip to reach 90% of the value at beam end. As expected, larger interface slip occurred in models with smaller degree of composite action. For models 6-UPN65X50, 4-UPN65X100, and 5-UPN65X75 even though the degree of composite action is larger than unity, there is still relative slip of 1-2 mm between the concrete slab and the steel beam at the interface. This observation, which is attributed to insufficient stiffness of shear connectors, agrees with the lack of strain compatibility between the concrete and the steel at the interface, as explained in the previous section.

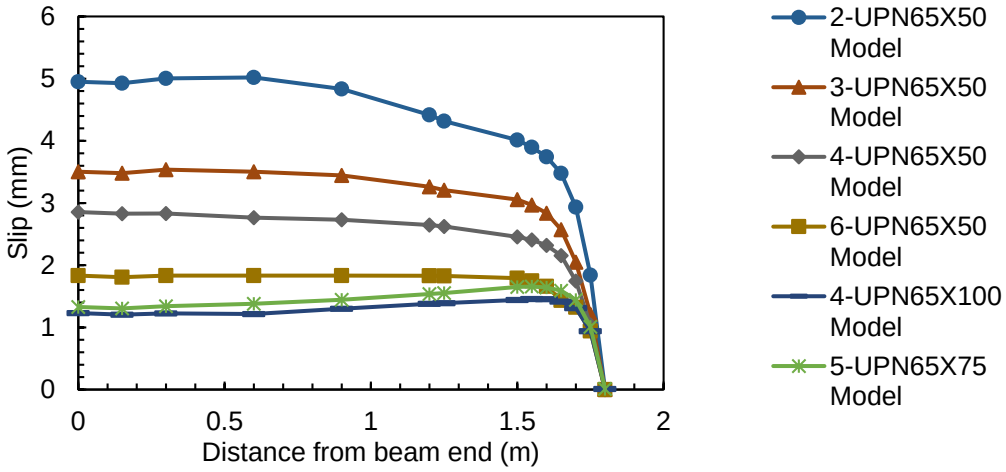

Figure 3.10. Variation of interface slip along beam length at 75 mm midspan deflection

A comparison of the measured interface slip values in composite beam specimens tested by Baran and Topkaya (2014) with those numerically obtained in the current study from the OpenSees models is provided in Fig. 3.11. The interface slip values measured at both ends of each beam specimen is given in these plots. Due to the absence of a perfect symmetry condition in test beams, the slip values measured at both beam ends usually differ from each other. For numerical models, on the other hand, the interface slip at both ends are always equal to each other due to the symmetry in geometry and loading with respect to the beam midspan section. The plots show the general trend of decreasing end slip with increasing level of composite action. The numerical model is able to predict the beam end slip accurately, except for model 4-UPN65X100. The discrepancy between the measured and predicted end slip values for the case of 4-UPN65X100 is believed to be due to inaccurate slip measurement during load testing of specimen 4-UPN65X100. This specimen was one of the three full composite beams tested by Baran and Topkaya (2014) and the measured end slip values for this beam are larger than those for the other two fully composite beams. The discrepancy in the experimental results may be attributed to the factors such as uplift that may took place during load testing or due to imperfect steel-concrete interface in the specimen.

As explained earlier, the numerical models indicate that the interface slip values increase rapidly starting from the midspan section and reach to an almost constant value after a certain distance. The reason for such distribution of slip along beam length is due to the concentrated midspan loading used in test beams and in numerical models. In order to study the effect of vertical shear force diagram on the variation of interface slip along beam length, model 6-UPN65X50 was further analyzed under uniformly distributed loading. The slip profiles along beam length obtained for the cases of midspan concentrated loading and uniformly distributed loading at a midspan deflection of 75 mm are compared in Fig. 3.12. As opposed to the midspan concentrated loading case, the uniformly distributed loading results in a gradually increasing interface slip along beam length. The shape of the slip profile along beam length is closely related with the shape of the vertical shear force diagram. The gradually increasing slip profile obtained for the case of uniformly distributed

loading is due to the fact that this type of loading creates a shear force diagram starting at midspan section and increasing linearly toward beam ends.

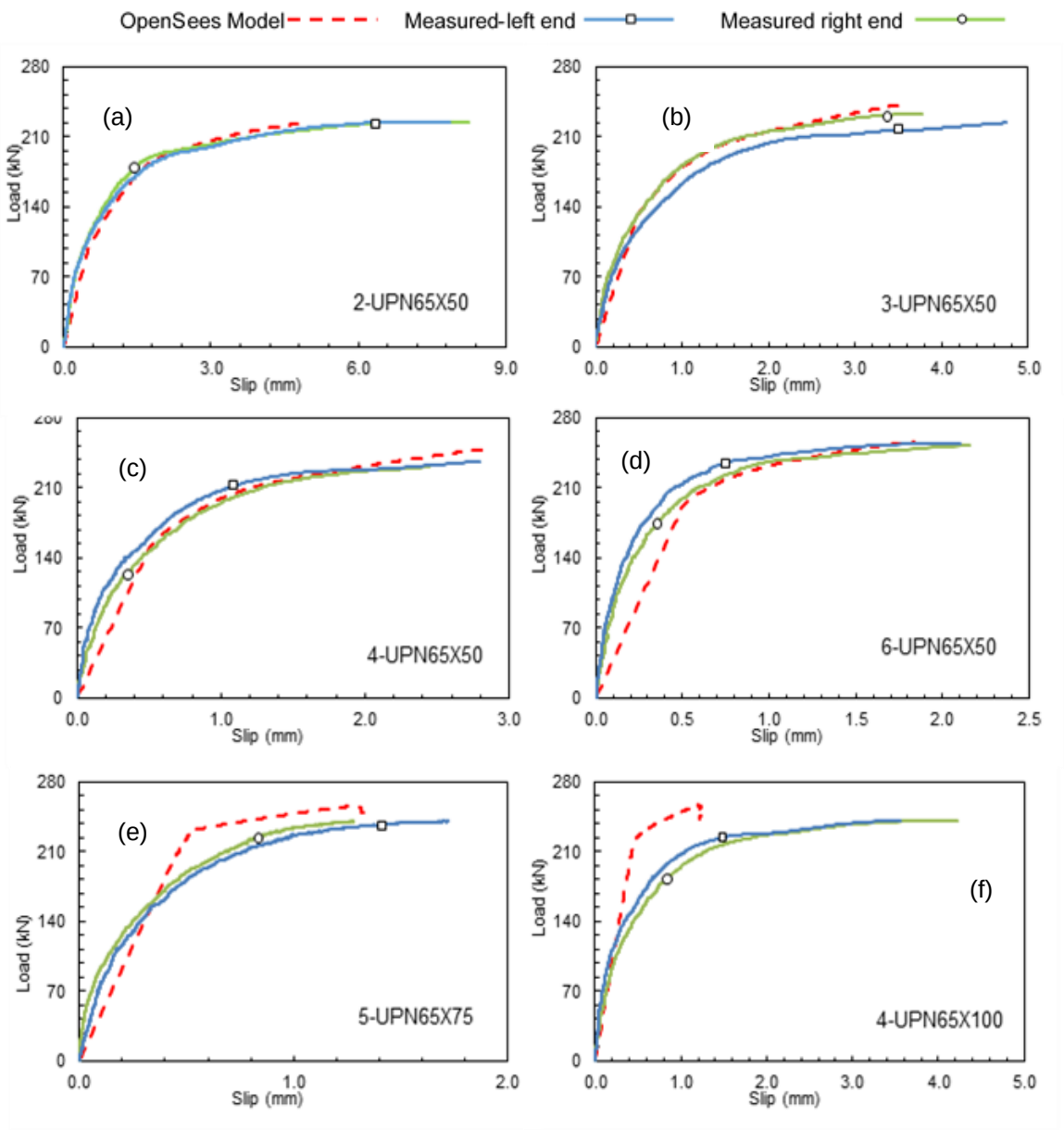

Figure 3.11. Comparison of measured and predicted beam end slip

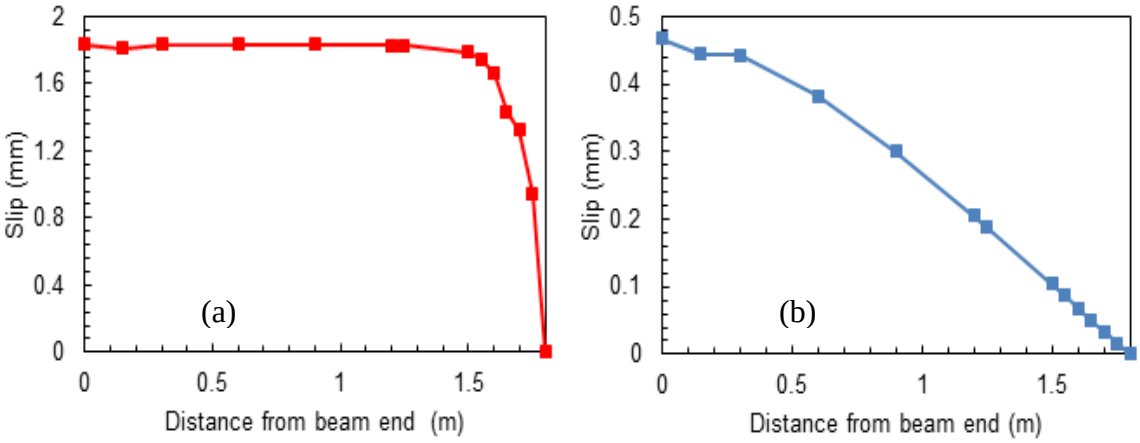

Figure 3.12. Variation of interface slip along beam length for model 6-UPN65X50: (a) concentrated load; (b) uniformly distributed load

The results of the analysis models in terms of slip profile were also verified by the analytical solution available in the literature. Viest et. al. (1997) provided a closed form solution for the interface slip in the case of partial composite interaction and under the effect of uniformly distributed loading. The slip *s(x)* under a uniformly distributed load *q* is obtained using Eq. 3.6.

$$s(x) = \frac{q.h}{\alpha^3.EI_{abs}}\left[\frac{1-\cosh(\alpha l)}{\sinh(\alpha l)}\right].\cosh(\alpha x) + \sinh(\alpha x) + \frac{\alpha l}{2} - \alpha x \qquad \text{(Eq.3.6)}$$

In the equations provided below, *EA* is the axial stiffness and *EI* is the flexural stiffness of each material, k_s is the stiffness of the shear connector, and *h* is the distance between the centroids of the concrete and steel parts. The necessary parameters such as EA_{eq}, EI_{abs}, EI_{full} and α are obtained from Eqs. 3.7 to 3.10.

$$EA_{eq} = \frac{(EA)_c(EA)_S}{(EA)_c+(EA)_s} \qquad \text{(Eq.3.7)}$$

$$EI_{abs} = (EI)_c + (EI)_s \qquad \text{(Eq.3.8)}$$

$$EI_{full} = EI_{abs} + EA_{eq}.h^2 \qquad \text{(Eq.3.9)}$$

$$\alpha^2 = \frac{k_s\, EI_{full}}{EA_{eq}.EI_{abs}} \qquad \text{(Eq.3.10)}$$

Figure 3.13 shows the interface slip profiles along the beam length for the cases 300 mm and 100 mm shear connector spacing. Uniformly distributed load with a nominal value of 0.01 kN/mm applied on the beam in model 6-UPN65X50. The applied load is kept small in order to make sure that the materials and the shear connectors remain in the linear elastic range. This is required for a proper comparison because the closed form solution considers only linear elastic properties for the concrete and steel parts, as well as the shear connectors. The remarkable agreement between the slip profiles from the analytical expression and from the OpenSees model is evident in plots shown Fig. 3.13.

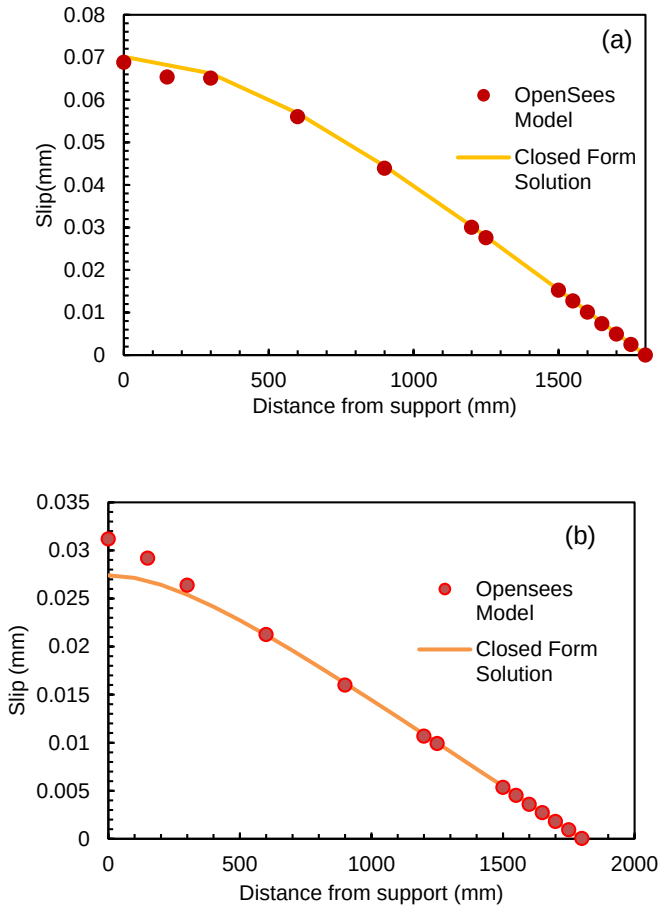

Figure 3.13. Comparison of predicted interface slip with analytical solution for (a) 300 mm connector spacing ; (b) 100 mm connector spacing

3.6 EFFECT OF SHEAR CONNECTOR LOCATION

In current design specifications, the position of shear connectors within shear span is not considered as a parameter affecting the behavior of composite beams. Further analyses were conducted using the Opensees model in order to study the effect of connector location on response of composite beams. For this purpose, a single UPN65X50 channel shear connector was placed symmetrically on either side of beam midspan and the location of this connector was varied. The analyses were repeated for both midspan concentrated loading and uniformly distributed loading cases. The load-deflection response corresponding to different locations of channel shear connectors are plotted in Figs. 3.14 and 3.15. Results from both loading cases reveal the general trend that the initial elastic stiffness and load capacity of beam increases as the shear connector is placed closer to the beam end. The definition in AISC 360-10 (2010) for partial degree of composite action only considers the strength of shear connectors without any consideration of the location of these connectors. The analysis results, however, clearly indicate the dependence of beam stiffness and strength on shear connector location.

Another observation that is valid per Figs. 3.14 and 3.15 is that for the midspan concentrated loading case placing the shear connector at beam ends and 1000 mm from midspan does not cause any appreciable difference on the load-deflection response. This is due to the fact that with this type of loading the interface slip increases rapidly in the vicinity of midspan section and remains almost constant for the rest of the beam. Therefore, as long as the shear connector is located within the region where the interface slip does not change significantly, the exact location of the connector does not cause significant difference in the overall beam response. The same observation is not valid, however, for the distributed loading case because starting from the midspan section the interface slip increases continuously until beam ends.

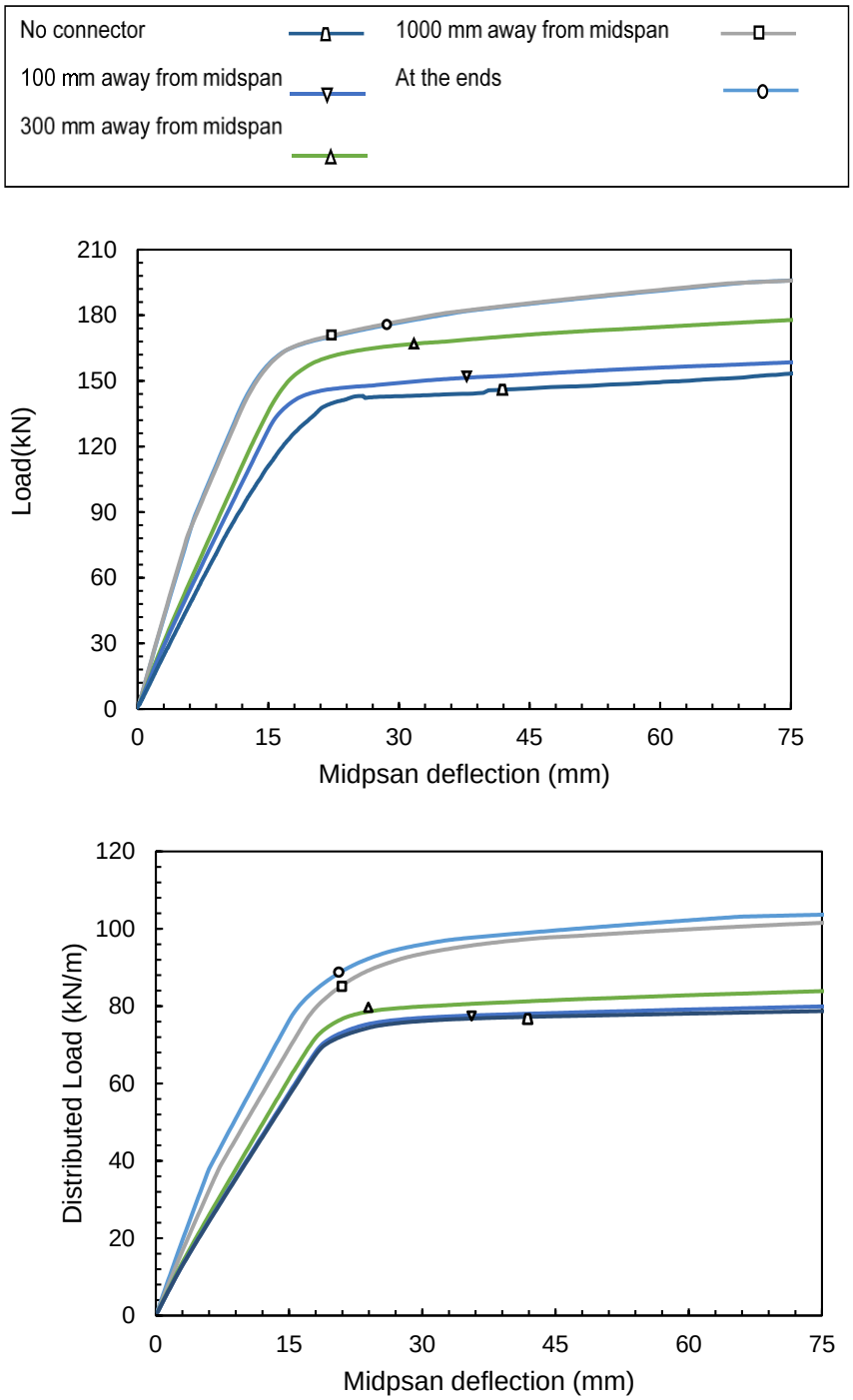

Figure 3.14. Load vs. midsplan deflection for different connector locations (a) concentrated load (b) distributed load

CHAPTER 4

CONCLUSIONS

In this thesis, flexural response of partially composite beams with channel type mechanical shear connectors were studied numerically. A detailed finite element model was developed in OpenSees framework employing displacement-based beam-column elements with the fiber approach. The interaction between steel beam and concrete slab was accounted for by introducing nonlinear zero length elements and rigid links. The channel shear connector response used in numerical models was based on the previously obtained experimental response from pushout tests (Baran and Topkaya, 2012).

A total of six composite and one bare steel beam models were analyzed. Accuracy of the numerical models in predicting the response of partially composite beams was verified with the results of the previously conducted composite beam tests (Baran and Topkaya, 2014). The numerically determined load versus midspan deflection response was compared with the experimentally obtained response both for fully composite and partially composite beams and predicted response was observed to agree well over the entire range of load-deflection curves.

The numerical models were also able to accurately predict the interface slip between steel beam and concrete slab when compared to the experimentally determined slip values, as well as the closed form slip predictions.

The numerical results indicated that the load capacity from the simple code procedure underestimates the capacity of partially composite beams, while the load capacity of fully composite beams is slightly overestimated.

The effective and lower bound moment of inertia values as defined by the AISC 360-10 Specification resulted in overestimation of beam stiffness for all degrees

of composite action studied. On the other hand, reducing the effective moment of inertia by 25% matched the numerically obtained elastic beam stiffness values fairly well.

Concrete cracking in slab was observed to start at very early stages of loading and progress very quickly irrespective of the degree of composite action. The initiation and progression of concrete cracking did not cause a major influence on load-deflection response of beams. Concrete cracking was followed by the initiation of yielding at bottom part of steel beam. Yielding in lower parts of steel beam was observed to be more extensive in models with full composite action compared to the partially composite beams. The extent of yielding in compression part of steel beam, on the other hand, was larger in models with smaller degree of composite action. Crushing of concrete slab occurred to some extent only in fully composite beams, which is an indication of increased compression demand on concrete slab with increasing strength and stiffness of interface shear connectors.

The point that the initial portion of the load-deflection curve of composite beams deviates from linear response corresponded to yielding of the entire bottom flange of steel beam. Therefore, it can be concluded that linear load-deflection behavior continues until the full yielding of beam bottom flange, rather than the initiation of yielding as would be expected.

Partially composite behavior revealed itself in the form of a discontinuity in cross-sectional strain profile at steel-concrete interface. Such a discontinuous strain profile was also obtained for fully composite beams, indicating a nonzero slip between the concrete slab and the steel beam at the interface. Such a lack of strain compatibility was an indication that even the total horizontal shear force capacity of connectors provided at the interface is sufficient to develop full yielding of the steel beam or crushing of the concrete slab, this condition does not guarantee a no-slip case and hence a continuous strain profile. The magnitude of interface slip and the extent of strain compatibility between the concrete slab and the steel beam are dictated by the stiffness of the shear connectors, as well.

The numerical results showed the general trend that the initial elastic stiffness and load capacity of beam increases as the shear connector is placed closer to the beam

end. The definition in AISC 360-10 (2010) for the partial degree of composite action only considers the strength of shear connectors without any consideration of the location of these connectors. The analysis results, however, clearly indicated the dependence of beam stiffness and strength on shear connector location.

REFERENCES

AISC. Specification for structural steel buildings. Chicago (IL): AISC-360-10, American Institute of Steel Construction; 2010.

Baran E, Topkaya C. An experimental study on channel type shear connectors. J Constr Steel Res 2012; 74:108–17.

Baran E, Topkaya C. Behavior of steel-concrete partially composite beams with channel type connectors. J Constr Steel Res 2014; 97:69 –78.

Chiorean CG, Buru SM. Practical nonlinear inelastic analysis method of composite steel-concrete

beams with partial composite action. Engineering Structures 2016; 134:74-106.

CSA. CAN/CSA-S16-01 Limit States Design of Steel Structures, including CSA-S16S1-05 Supplement No. 1. Canadian Standard Association, Toronto, ON; 2001.

Dall'Asta A, Zona A. Non-linear analysis of composite beams by a displacement approach. Computers and Structures 2002; 80:2217-2228.

Design of beams in composite bridges (2012, June). Retrieved from http://www.steelconstruction.info

El-Lobody E., Finite element modelling of shear connection for steel-concrete composite girders, PhD thesis, The University of Leeds, Leeds; 2002.

BS EN 1992-1-1. Design of concrete structures – Part 1-1: General rules and rules for buildings. Brussels: BS EN 1992-1-1, European Committee for Standardization (CEN); 2004.

Griffis L.G. Some design considerations for composite-frame structures. Engineering Journal 23 1986; 23(2):59-64.

Jiang A, Chen J, Jin W. Experimental study of innovative steel-concrete composite beams under hogging moment. Advances in Structural Engineering 2013; 16:877-886.

Jurkiewiez B, Maeud C, Ferrier E. Non-linear models for steel-concrete epoxy-bonded beams. J Constr Steel Res 2014; 100:108-121.

Lin W, Yoda T. Numerical Study on Horizontally Curved Steel-Concrete Composite Beams Subjected to Hogging Moment. International Journal of Steel Structures 2014; 14(3):557–569.

Majdi Y, Hsu CT, Zarei, M. Finite element analysis of new composite floors having cold-formed steel and concrete slab. Engineering Structures 2014; 7:65-83.

Maleki S, Bagheri S. Behavior of Channel Shear Connectors, Part II: Analytical Study, J Constr Steel Res 2008; 64:1341-1348.

McKenna FT. Object-Oriented Finite Element Programming: Frameworks for Analysis,Algorithms and Parallel Computing, PhD thesis, University of California, Berkeley; 1997.

Muhit IB. Various types of shear connectors in composite structures. Technical note, Chung-aung University, Seoul; 2015.

Newmark NM, Siess CP, Viest IM. Tests and analysis of composite beams with incomplete interaction. Proceedings of the Society of Experimental Stress Analysis 1951; 9(1):75-92.

Nie JG, Fan J, Cai CS. Experimental study of partially shear-connected composite beams with profiled sheeting. Engineering Structures 2008; 30:1-12.

Oehlers DJ, Bradford MA. Composite steel and concrete structural members: fundamental behaviour, Pergammon, 1995.

Opensees. Version 2.0 user command-language manual, 2009.

Pashan A, Hosain MU. New design equations for channel shear connectors in composite beams. Can J Civil Eng 2009; 36:1435–43.

Pathirana SW, Uy B, Mirza O, Zhu X. Flexural behaviour of composite steel-concrete beams utilising blind bolt shear connectors. Engineering Structures 2016; 114:181-194.

Queiroza, FD, PCGS. Vellascob, Nethercot DA. Finite element modelling of composite beams with full and partial shear connection. J Constr Steel Res 2007; 63:505–521.

Ranzi G, Zona A. A steel–concrete composite beam model with partial interaction including the shear deformability of the steel component 2007; 29:3026-3041.

Rios JD, Cifuentes H, Concha AM, Reguera FM. Numerical modelling of the shear-bond behaviour of composite slabs in four and six-point bending tests. Engineering Structures 2017; 133:91-104.

Salari MR, Spacone E, Shing PB, Frangopol DM. Nonlinear analysis of composite beams with deformable shear connectors ASCE J Struct Eng 1998; 124(10):1148-1158.

Shariati M, Sulong NHR, MM Arabnejad KH, Mahoutian M. Shear resistance of channel shear connectors in plain reinforced and lightweight concrete. Scientific Research and Essays 2011; 6(4): 977-983.

Vianna JC, Costa-Neves LF, PCGS Vellasco, SAL Andrade. Structural behaviour of T-Perfobond shear connectors in composite girders: An experimental approach. Engineering Structures 2008; 30(9): 2381-2391.

Viest IM, Colaco JP, Furlong RW, Griffis LG, Leon RT, Wyllie LA. Composite construction design for buildings. New York: McGraw–Hill; 1997.

Wang S, Tong G, Zhang L. Reduced stiffness of composite beams considering slip and shear deformation of steel J Constr Steel Res 2017; 131:19-29.

Zsarnóczay, Á. Experimental and Numerical Investigation of Buckling Restrained Braced Frames for Eurocode Conform Design Procedure Development, PhD thesis, Budapest University of Technology and Economics, Budapest; 2013.